AAS-JAKOBSEN COWI Multiconsult

JOHS HOLT AkerSolutions entail NGI DISSING+WEITLING architecture a|s mossmaritime

MEMO

PROJECT	Concept development, floating bridge E39 Bjørnafjorden	DOCUMENT CODE	10205546-11-NOT-212
CLIENT	Statens vegvesen	ACCESSIBILITY	Restricted
SUBJECT	K11 - Feasibility study for damper between tower and bridge girder, phase I	PROJECT MANAGER	Svein Erik Jakobsen
TO	Statens vegvesen	PREPARED BY	Mads Fredrik Heiervang / Per Norum Larsen / Knut Andreas Kvåle
COPY TO		RESPONSIBLE UNIT	AMC

CONTENT

This note describes the phase 1 of a feasibility study for a damper between tower and bridge girder. For this alternative K11 concept it is proposed to replace the girder-tower connection in K11_07, by two passive viscous dampers between tower and bridge girder. The viscous dampers are placed below the cross section, to minimize the necessary broadening of the tower. The modified tower is designed with a bottom leg spacing of 54m in order to accommodate for the lateral displacement amplitude of approximately 1.7m. A free span back span length of 305m is selected in order to increase the flexibility of the girder at the tower position, based on parameter studies for different free-span back span lengths.

Numerical analyses of the proposed design measure have been simulated in Orcaflex, and the response has been compared to the response of the K11_07. The results show that the strong axis moment swell response may be reduced by approx. 70%, and the axial force swell response may be reduced by approx. 30%, and the wind response is reduced by approx. 10%.

A robustness check of the concept with respect to global buckling has been performed, as the bridge may be vulnerable to static global buckling of the asymmetric buckling mode. Conservatively chosen extreme asymmetric load cases for wind and current has been applied with load factor, indicating that the analysed model has the necessary static resistance for this failure mode.

The dampers are characterized by a constant coefficient, c, and a velocity exponent, α. It is assumed that a linear damping characteristic, $\alpha = 1$, is preferable partly due to parametric excitation. Based on the initial dialogue with suppliers, the dampers should be feasible to construct with the desired/necessary characteristics.

A brief discussion of the selection of the parameters involved in a damper dashpot is included. By conducting a modal analysis of the different back-span configurations and with varying damper constants, ranges maximizing the modal critical damping ratios of relevant modes were established. The findings from these analyses indicate that a damper constant in the range 15–20 MNs/m is effective for the critical modes, when the bridge is excited by swell excitation. The risk of parametric excitation is assessed by evaluating the onset criterion, which is given in the document SBJ-32-C4-NTNU-22-RE-001 by the client and NTNU, provided at the outset of the project. A significant improvement of the robustness with respect to parametric excitation is observed from the inclusion of the damper; the critical axial force is increased from 5.6MN to 40.4 MN, and the bridge thus passes the onset criterion by a large margin. The standard deviation of the axial force due to a 100-year swell condition is 4.5MN. To assess the validity of the simplified approach for the parametric excitation analyses, the complexness and coupledness of the modes are evaluated. The findings support that the approach is reasonable.

0	27.04.2020	K11 - Feasibility study for damper between tower and bridge girder, phase I	MFH/KAK	Per Norum Larsen	Per Norum Larsen
REV.	DATE	DESCRIPTION	PREPARED BY	CHECKED BY	APPROVED BY

TABLE OF CONTENTS

1 Overview

The end-anchored floating bridge concepts for Bjørnafjorden have long eigenmodes with low damping, which results in relatively high response and the bridge may be vulnerable for parametric resonance. This memo contains a preliminary evaluation of a proposed design measure for the floating bridge crossings of Bjørnafjorden. By releasing the lateral constraint of the bridge girder at the tower and in the back-spans, the bridge girder can vibrate at the tower position. This allows for dashpots to be positioned at the connection to the tower, to introduce linear damping in the system. Thus, the critical damping of the longest transverse eigenmodes can be increased in order to ensure that (i) parametric resonance is avoided and (ii) the resonant swell response is limited.

In the analysis, a single dashpot system has been modelled between the tower and the bridge girder. However, in design it is proposed to use two linear viscous dampers as illustrated in Figure 1-2. The oscillating periods of the dashpots is listed in Table 2-5. If this option is considered further, we recommend contacting manufacturers for evaluation of constructability.

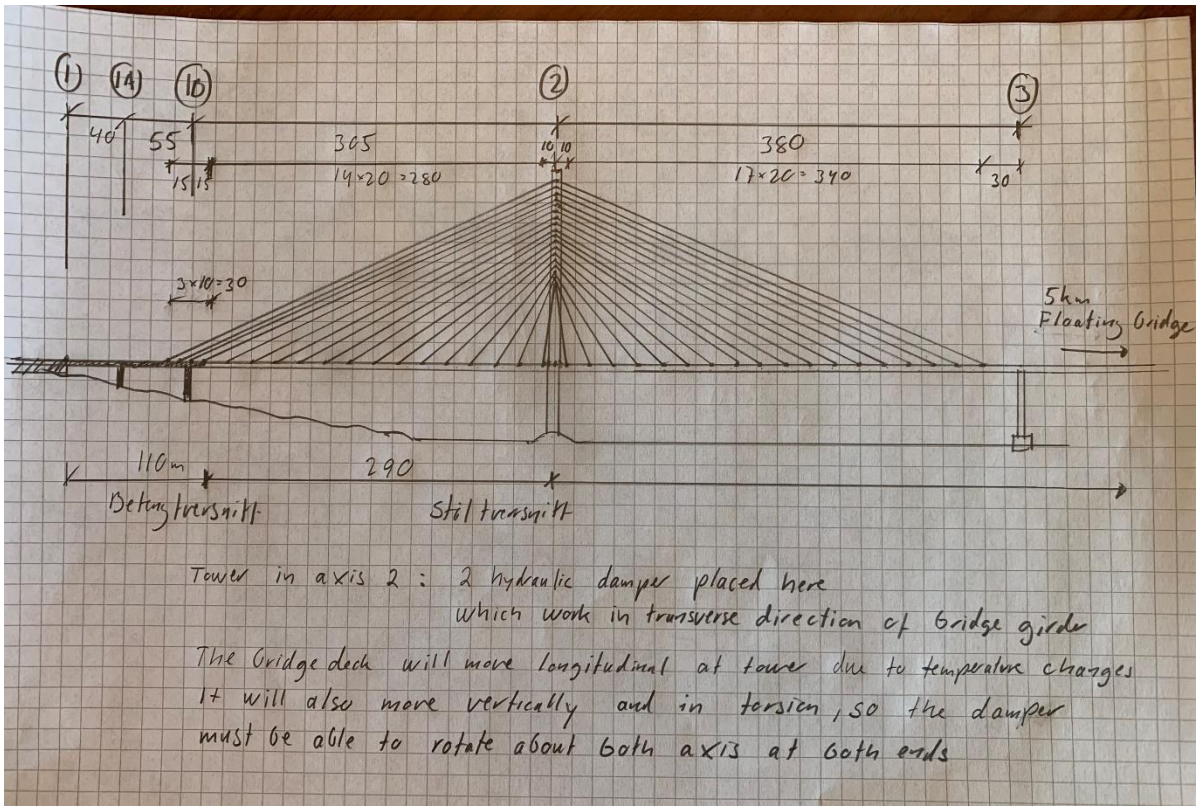

Figure 1-1 Illustration of proposed design for the K11 concept with tower damper. The back columns proposed for K11 at 1E, 1D and 1C has been replaced by a longer cable-stayed back-span to increase the transverse flexibility of the bridge at axis 2, such as to better mobilise the hydraulic dampers.

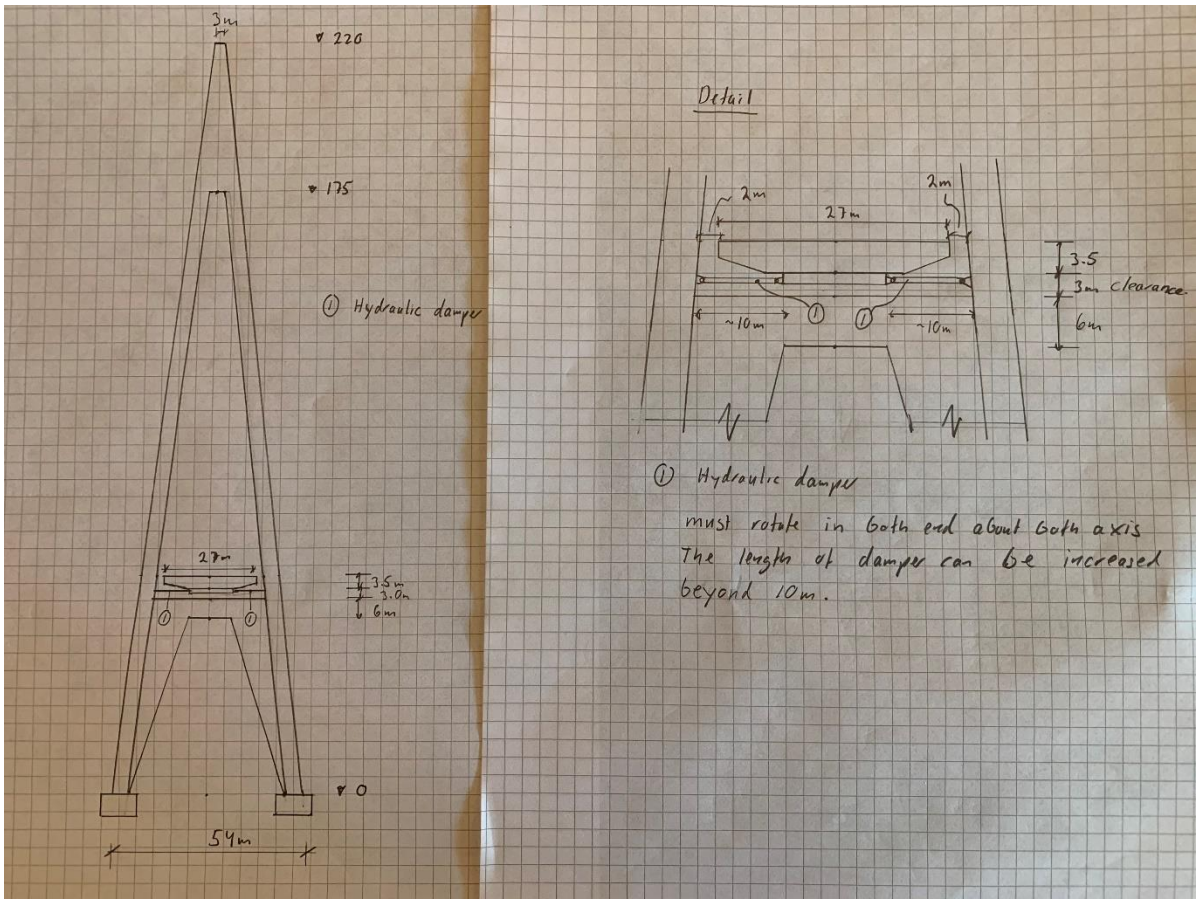

Figure 1-2 Illustration of the adjusted tower and indicative placement of the two hydraulic dampers between tower and bridge girder. The tower is adjusted to obtain sufficient clearance between bridge girder and tower, to allow for damper displacement.

The dampers are typically delivered with a c-coefficient and an α factor given by the following expression:

$$f_d = c \cdot V^{\alpha}$$

where f_d is the damping force and V is the relative velocity between the two ends of the damper. The selected damper has a linear damper characteristic ($\alpha = 1$) and $c = 15$ MNs/m.

Table 1-1: Summary of characteristic 100 year response for the selected damper between bridge girder and tower.

	Amplitude		***Velocity***	***Period***	***Load***
	Mean	***Expected max***	***Expected max***	***-***	***Expected max***
Swell	*0*	*0.21m*	*0.09m/s*	*17s*	*1.3MN*
Windsea		*0.23m*	*0.25m/s*	*6.2s*	*3.8MN*
Dynamic Wind	*0*	*0.7m*		*-*	
Static Wind	*0.7m*				
Current	*0.3m*				
Temperature	*0.15m*				
Combined	*1.0m*	*1.7m*	*0.26m/s*	*17s*	*4.1 MN*

2 Global analysis

2.1 Model description

A numerical model has been established in Orcaflex, adapted from the K11 basecase model presented in Appendix F. The girder cross-sections are equivalent to K11_07, except for the back-span, where the concrete back-span has been replaced by the H1 cross section. For simplification, the girder is modelled as free to translate laterally in the back-span and supported in the back-span vertically, for illustration see Figure 2-1.

In the analyses the bridge girder has been supported vertically on the back-span columns, but free to translate laterally. Such a system may be difficult to design, but the columns may be replaced by a longer cable-stayed back-span. The effect of a cable-stayed system versus a column-supported system with gliding bearings has not been considered.

In the next phase for the feasibility study, a back-span without columns should be modelled. For the base case the rigid lateral connection between the tower cross beam and girder is replaced by a linear damper with c =15 MNs/m.

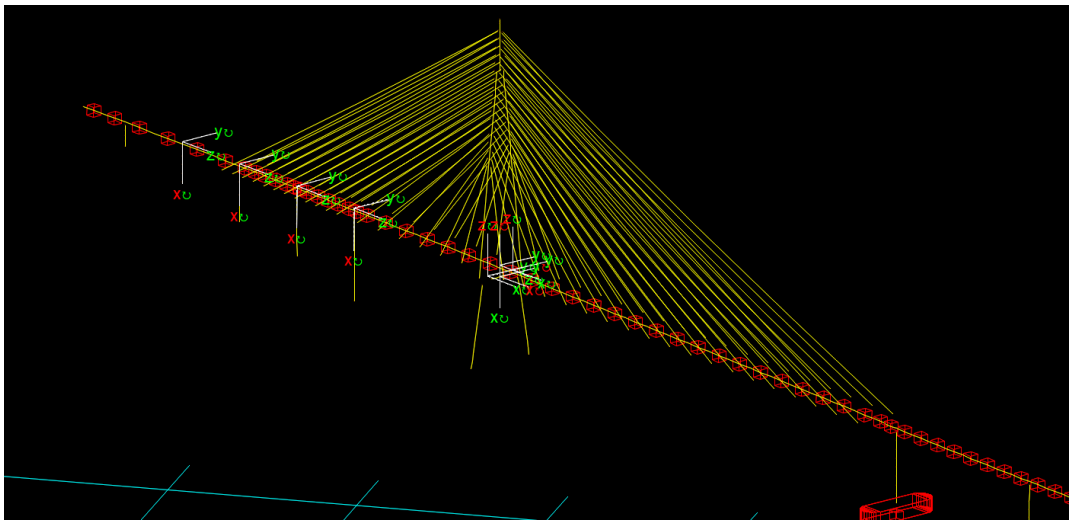

Figure 2-1: Snapshot of the cable-stayed tower part of the numerical model in Orcaflex

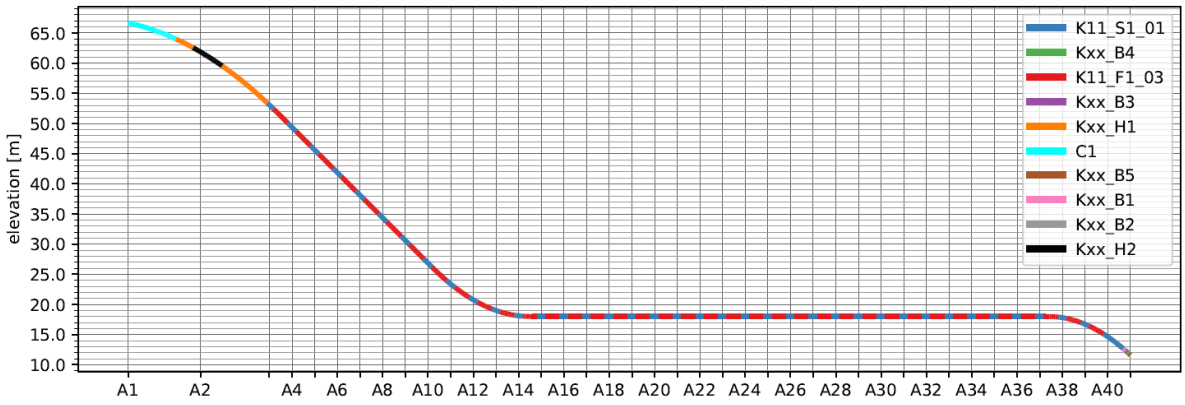

Figure 2-2: Cross-sections distributions in the bridge girder for K11_07. For the tower damper concept, the girder cross-sections are equivalent to K11_07, except for the back-span, where the concrete back-span (C1) has been replaced by the H1 cross section.

Table 2-1 Key sectional properties for K11_07.

	M	Iy	Iz	J	Ax	Ly	Lz	VCGt
	[tonne/m]	[m^4]	[m^4]	[m^4]	[m^2]	[m]	[m]	[m]
K11_S1_01	19.0	4.3	135.5	13.7	2.10	27	4	1.90
K11_F1_03	19.0	2.9	107.2	9.8	1.43	27	4	1.90
Kxx_H1	19.0	2.6	97.9	6.4	1.35	27	3.5	1.56
Kxx_H2	19.0	3.5	126.7	9.7	1.75	27	3.5	1.56
C1	79.1	40.5	2138	135	28.0	29	3.5	1.56
Kxx_B1	19.0	5.3	170.0	18.2	2.09	27	4	1.90
Kxx_B2	20.5	6.0	226.0	20.0	2.28	27	4	1.90
Kxx_B3	25.2	7.7	314.0	24.3	2.86	27	4	1.90
Kxx_B4	29.0	9.7	423.0	28.5	3.34	27	4	1.90
Kxx_B5	30.1	10.1	461.0	29.7	3.48	27	4	1.90

2.2 Environmental conditions

For comparison of the K11 basecase and the tower damper alternative the 100 year wind, windsea and swell conditions have been simulated in Orcaflex. The selected sea states are presented in Table 2-2 and Table 2-3.

Table 2-2: Selected design load cases for the 100year wind waves

	Design case 1
Hs [m]	2.1
Tp [s]	5.5
Wave Direction [deg]	70 / 105

Table 2-3: Selected design load case for the 100 and 10 000-year swell, based on the selected base case. Note that the swell conditions have been applied at the critical eigenmode for both the K11 basecase and the tower damper alternative.

	Design case 1	Design case 2
Hs [m]	0.34 / 0.46	0.34 / 0.46
Tp [s]	16.96	13.0
Wave Direction [deg]	300	305

Table 2-4: Wind spectrum characteristics

Parameter	**Value**
V_m at z=10m, 100-year / 10 000-year [m/s]	29.4 / 35.7
Adjustment factor for east direction (V_m)	0.85
A_u / A_v / A_w	6.8 / 9.4 / 9.4
L_1 / z_1	100 / 10
Coherence spectrum	N400
Length scale	N400
I_u / I_v / I_w	$1/ln(z/z_0)$ / $0.84I_u$ / $0.6I_u$
z_0	0.01

2.3 Parameter study for back-span length and damper coefficient

Selected results from the parameter study are presented in Table 2-5. The maximum strong axis bending moment in the bridge girder is reduced by 70% for the swell design case and the wind response is reduced by 10%. The axial force response in the bridge girder from swell is an important parameter for evaluation of parametric resonance. The axial force response of the tower damper alternative is reduced with roughly 30% as compared to the K11_07. See also Figure 2-4–Figure 2-9.

For the K11 tower damper alternative the horizontal translation at the location of the damper has been extracted, see Table 1-1. From the results it is estimated that the necessary length of stroke for the damper is a minimum of 1.7m in each direction, where 0.7m is the dynamic amplitude and 1.0 is the static offset.

At the tower there is a significant reduction of the dynamic strong axis bending moment as compared to the K11_07 design, which is also the case for the mean wind strong axis moment response, see Figure 2-10. This is partly due to the redistribution of forces as the girder is free to translate laterally at this position However, the redistribution results in a significant increase of bending moment towards the end abutment in south.

*Table 2-5: Selected 10 000-year results for parameter study of free-span back-span length and damper coefficient, as compared to the K11_07 design. The backspan length is denoted according to the column positions in Figure 2-3. The selected basecase for the tower damper concept is highlighted in **bold**. Note that the damper coefficient sensitivity is performed for A1 for wind, 1B for swell mode 5 and 1C for swell mode 6.*

Backspan	Damping	Dynamic wind SAM [MNm]			Swell Mode 5 SAM [MNm]			Swell Mode 6 A [MN]		
		A2	A9	A41	A2	A9	A41	A2	A9	A41
K11_07	**K11_07**	1100	730	1540	950	800	1300	-	-	-
A1	**0**	600	700	1480	170	1000	1600	30.5	30	28
A1	**15**	600	610	1300	170	220	375	24	23.5	22
A1	**20**	600	610	1300	170	220	375	23	22.5	21
A1	**25**	600	610	1300	170	220	375	22	21.5	20
A1	**15**	600	610	1300	170	220	375	23	22.7	21.4
1A	**15**	600	615	1325	169	240	390	23.3	23	21.7
1B	**15**	**600**	**620**	**1350**	**168**	**260**	**410**	**22.7**	**22.4**	**21.1**
1C	**15**	620	625	1375	167	280	440	22.5	22.2	20.9
1D	**15**	660	630	1400	166	300	480	22.7	22.4	21.1
1E	**15**	700	635	1425	165	320	550	23.6	23.3	22

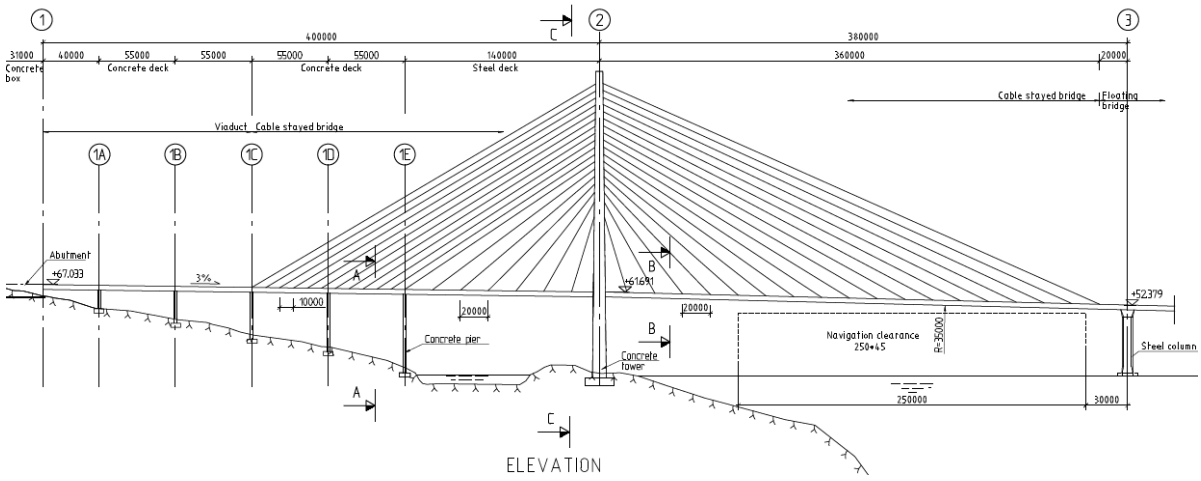

Figure 2-3: Side view of the K11_07 high bridge design, indicating position for the sensitivity of the back-span length.

Table 2-6: Eigenperiods for the first 9 eigenmodes for the different back-span lengths considered for the tower damper concept. Note that for the presented eigenperiods only the mass and stiffness matrices have been included in the modal analysis.

Mode number	A1	1A	1B	1C	1D	1E
1	115.1	115.1	114.9	114.6	114.0	113.3
2	61.2	61.2	61.0	60.8	60.5	60.2
3	34.7	34.7	34.6	34.4	34.1	33.9
4	23.7	23.7	23.6	23.5	23.3	23.2
5	17.1	17.0	16.9	16.8	16.7	16.6
6	13.1	13.1	13.0	13.0	13.0	13.0
7	12.6	12.6	12.6	12.5	12.5	12.4
8	10.1	10.0	10.0	9.9	9.8	9.8
9	9.4	9.4	9.4	9.4	9.4	9.4

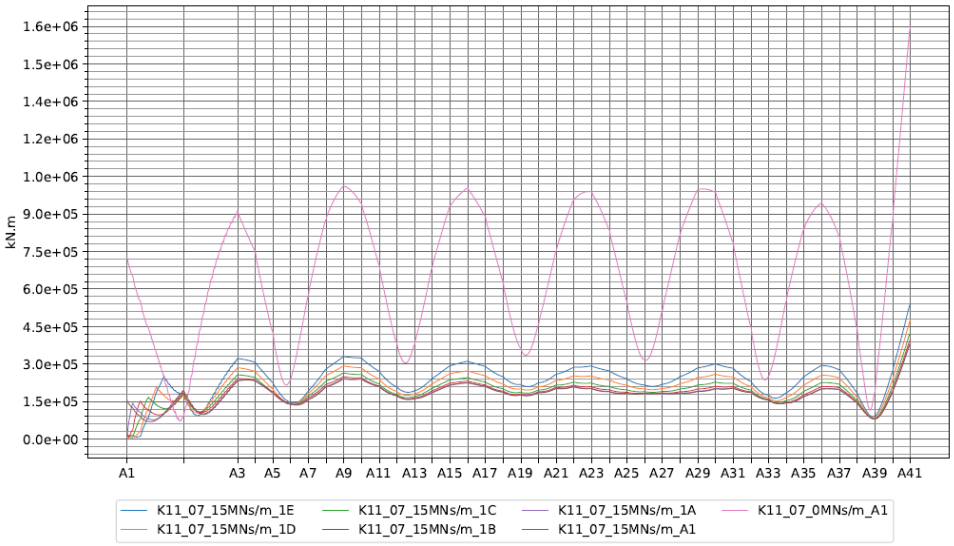

Figure 2-4: Parameter study of swell mode 5 strong axis moment for length of back-span. 10 000-year swell conditions has been applied for the parameter study.

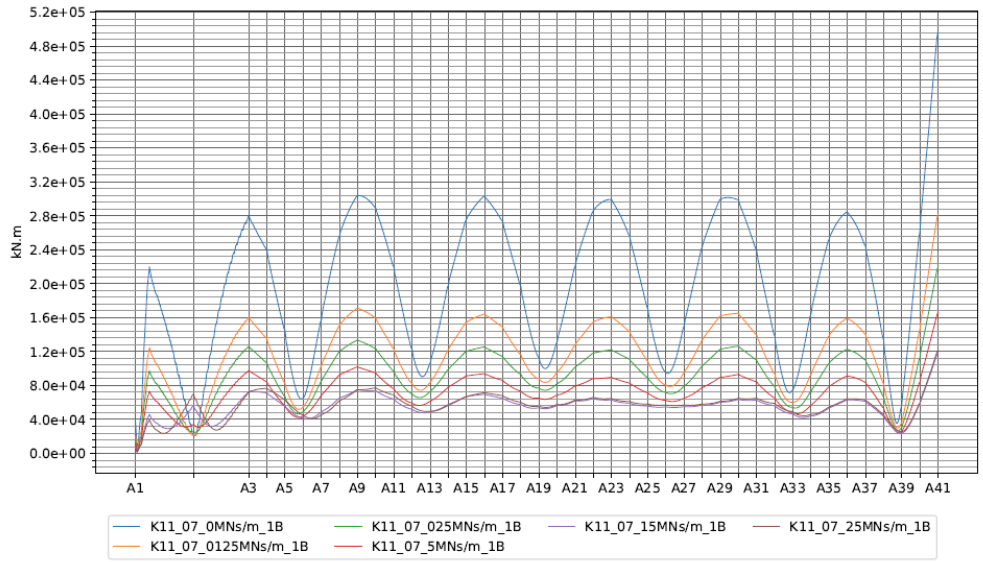

Figure 2-5: Parameter study of swell mode 5 strong axis moment response for damper coefficient. 10 000-year swell conditions has been applied for the parameter study.

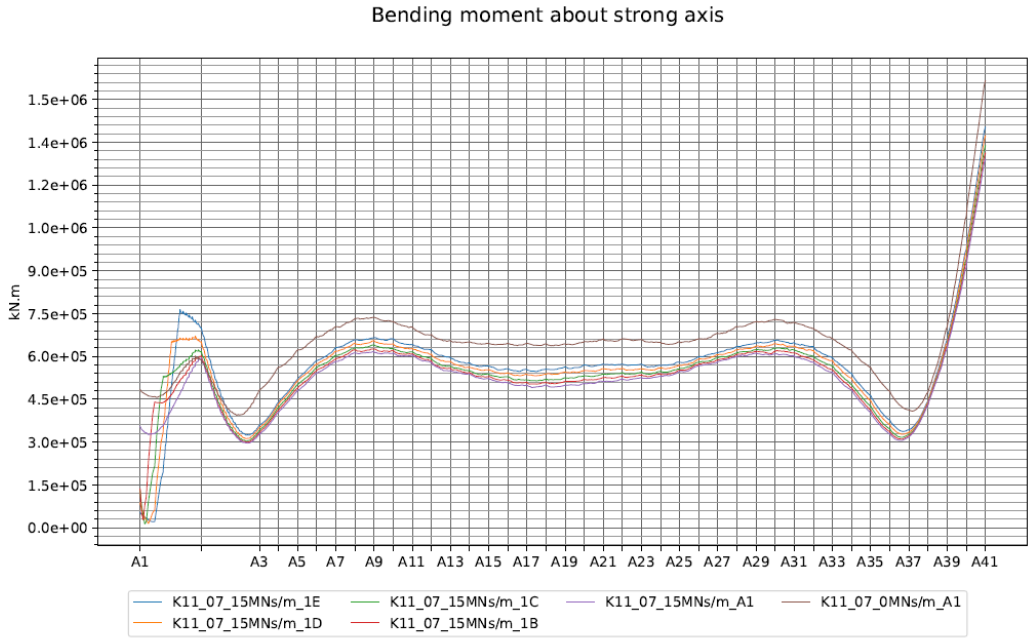

Figure 2-6: Parameter study of wind strong axis moment response for length of back-span. Wind from west has been used for the parameter study.

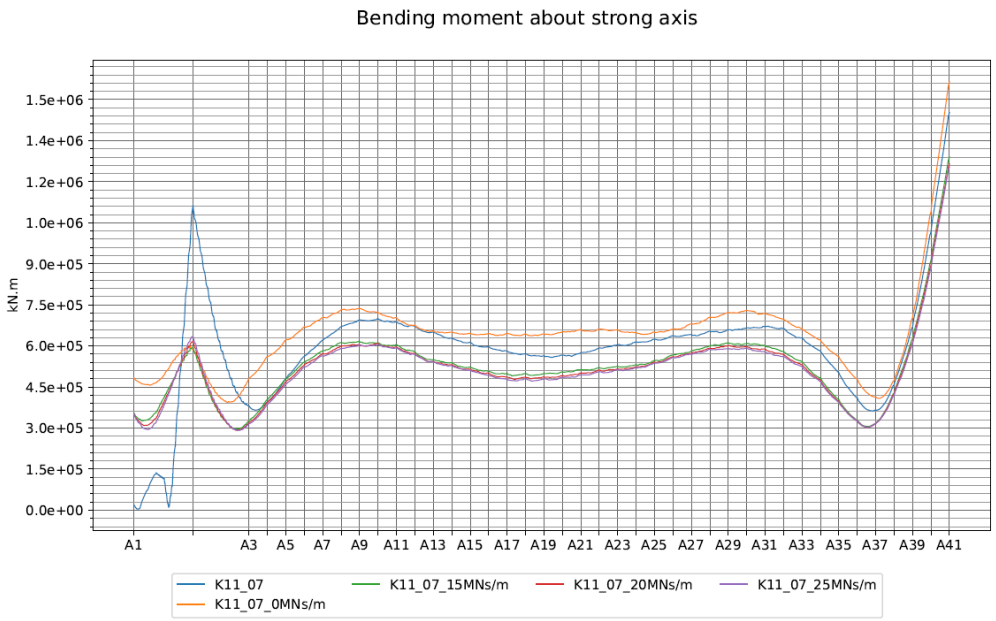

Figure 2-7: Parameter study of wind strong axis moment response for damper coefficient. Wind from west has been used for the parameter study.

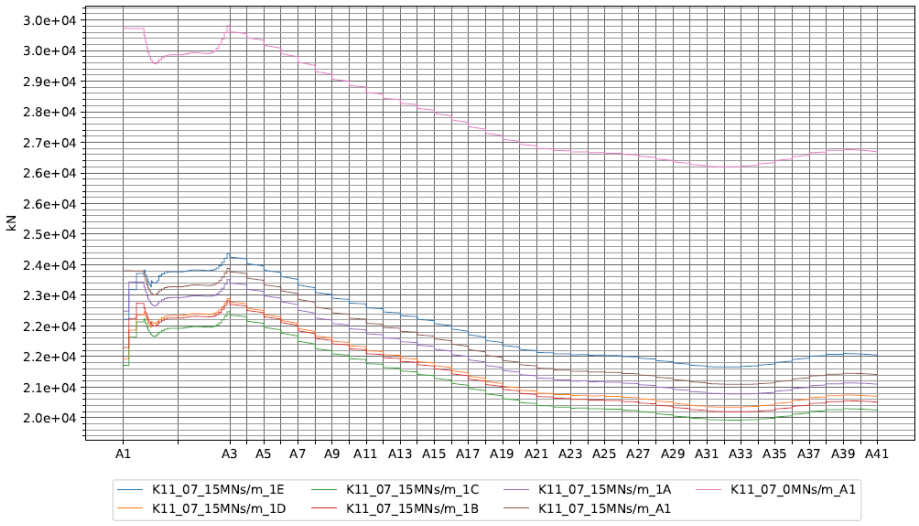

Figure 2-8: Parameter study of axial force from swell mode 6 for length of back-span. 10 000-year swell conditions has been applied for the parameter study.

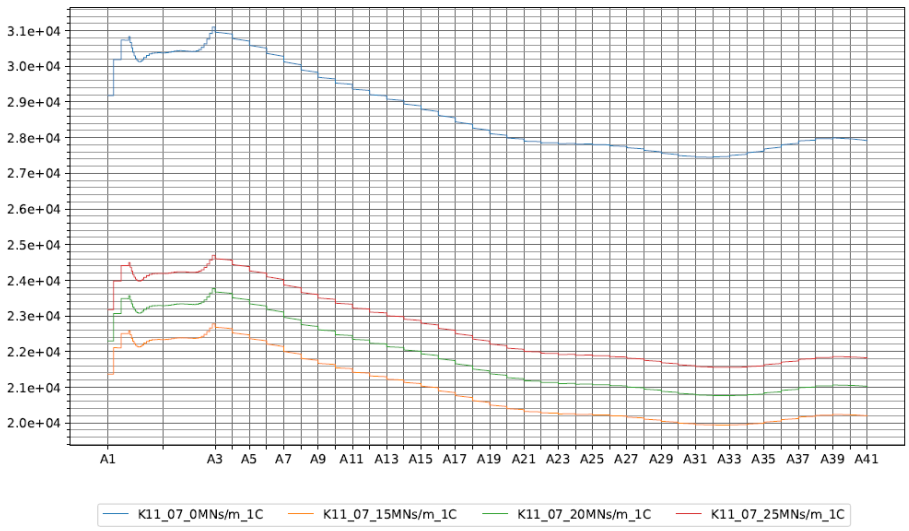

Figure 2-9: Parameter study of axial force from swell mode 6 for damper coefficients. 10 000-year swell conditions has been applied for the parameter study.

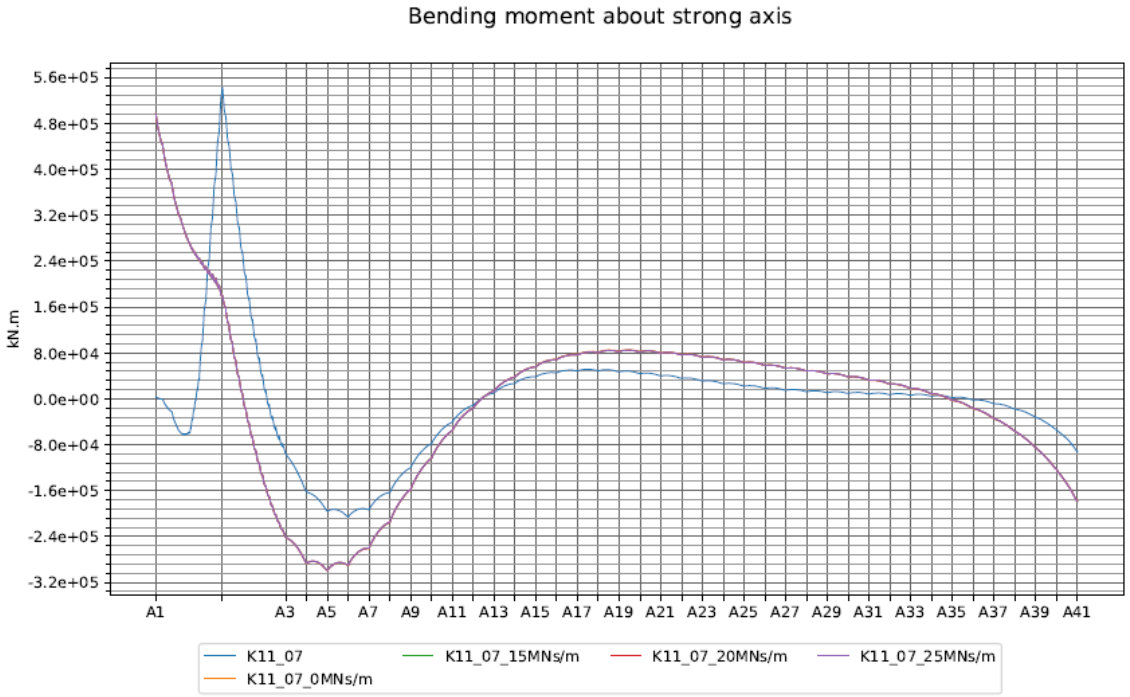

Figure 2-10: Mean wind strong axis moment response, considering 10 000-year condition from west

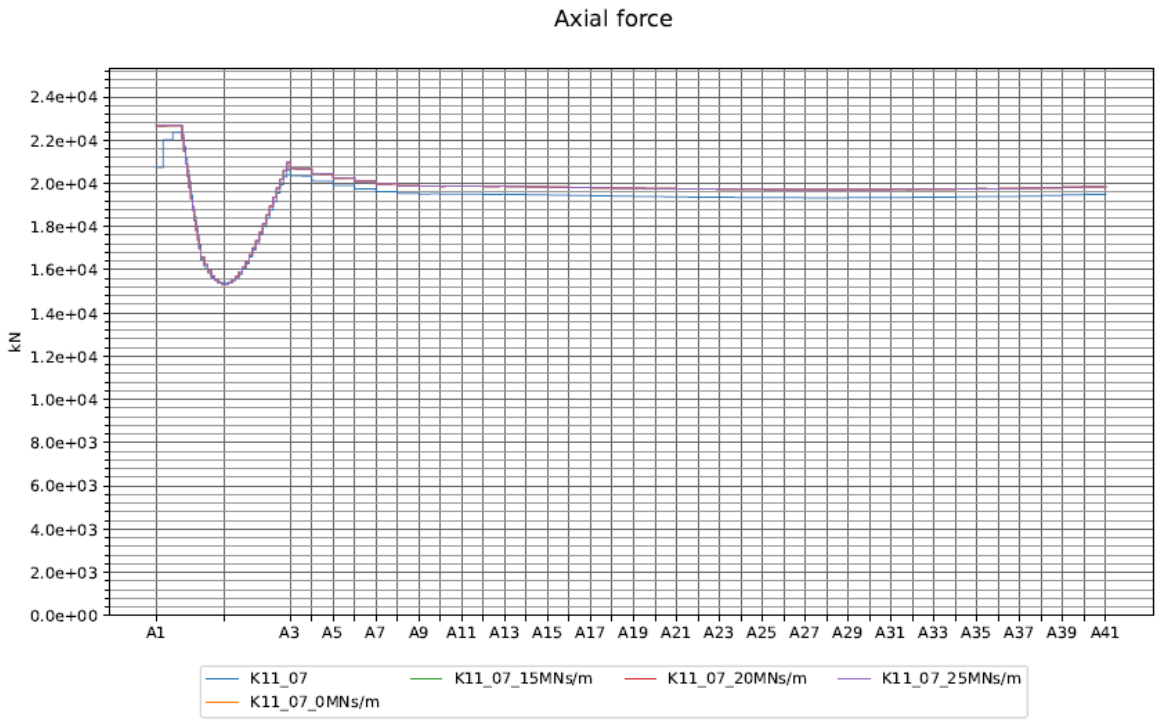

Figure 2-11: Mean wind axial force response, considering 10 000-year condition from west

2.4 Static resistance to global buckling

The K11 concept with a single steel box, a plan radius of 5000m and a distance between abutments of approximately 5000m between abutments, may be vulnerable to static global buckling of the asymmetric buckling mode. At this stage a set of conservative load conditions have been applied to evaluate the K11 tower damper concept's resistance to global buckling of the asymmetric case.

An inhomogeneous wind condition has been applied, with the 10 000-year extreme wind only applied on one half part of the bridge with load factors. The load condition is illustrated in Figure 2-12. Also, a 10 000-year current cross flow condition has been applied together with a homogeneous wind distributed load (even plan mean wind distribution). The current load condition is illustrated in Figure 2-13.

The results is presented in Figure 2-14–Figure 2-22. The inhomogeneous wind load case results in a significantly higher strong axis moment response as compared to the even wind case, even though the axial force is reduced by roughly half. Also, the current crossflow load case results in a significantly higher response than the even wind case, and for a load factor 3.6 the response is approximately equal to the uneven wind case. However, the current cross flow shows a more non-linear characteristic for an increased load factor. The girder's capacity is somewhere around 2.6GNm when also accounting for the permanent action.

The given cases are chosen conservatively, and these load cases, with 10 000-year conditions together with high load factors are considered too conservative. However, the presented results show that the design has satisfying robustness for both uneven wind and the crossflow current with wind cases, and can sustain a load factor of 2 for both extreme cases. *Note: a shape factor, e.g. due to construction tolerance has not been considered, however with the selected conservative load cases and the resulting deformations the evaluation is still overall assumed to be conservative.*

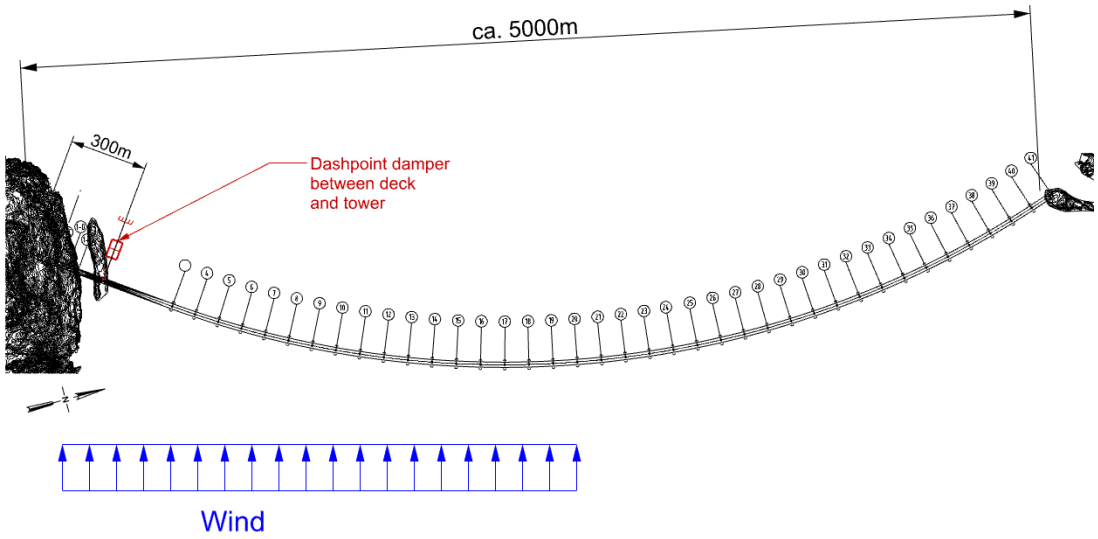

Figure 2-12: Illustration of wind distribution for the applied inhomogeneous wind case from east. This is assumed to be a conservative load case for the K11 concept, which is vulnerable for asymmetric load cases. Note that the distribution is for the mean wind velocity at a given height. The wind also varies with height, which is not illustrated here. The wind velocity has not been reduced, as compared to the extreme condition.

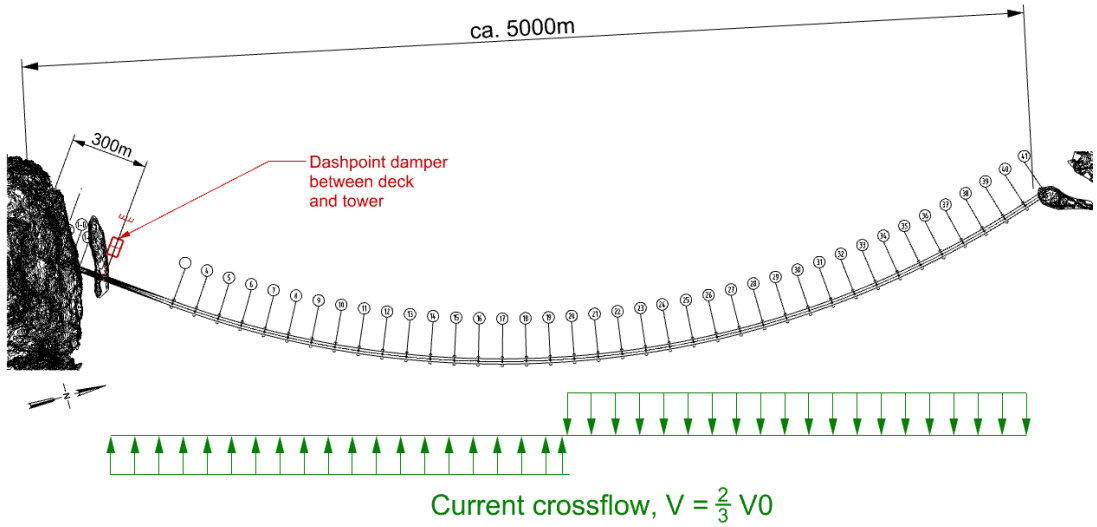

Figure 2-13: Illustration of current distribution for the applied cross flow case for current from east. This is assumed to be a conservative load case for the K11 concept, which is vulnerable for asymmetric load cases. Note that the current velocity does not vary with depth. V is 1.32m/s and V0 is ~2m/s for the 10 000-year condition from east.

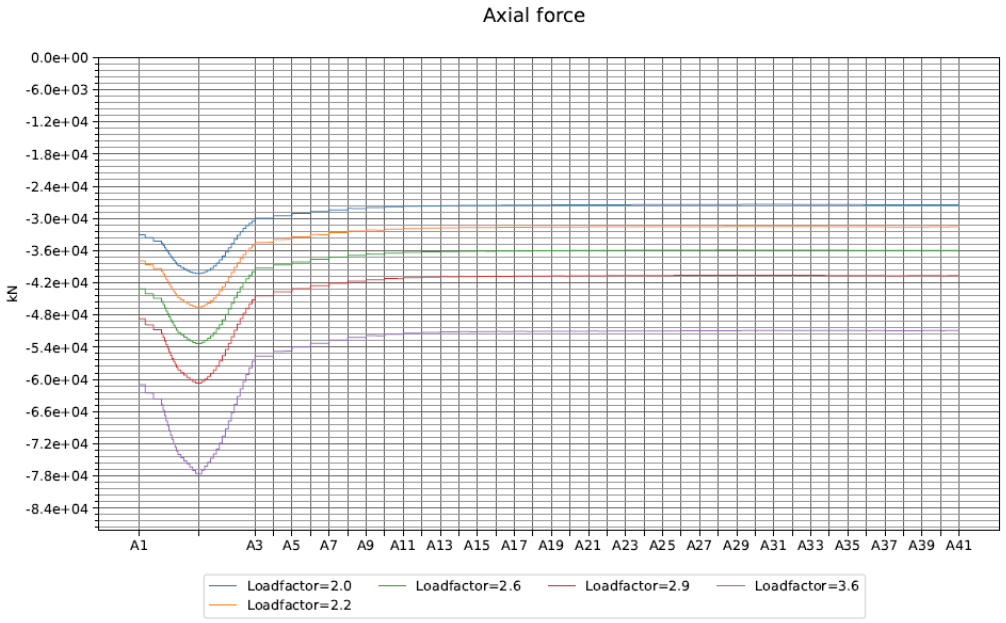

Figure 2-14: Static axial force response to 10 000-year wind conditions from east, homogeneous wind distribution with labelled load factors.

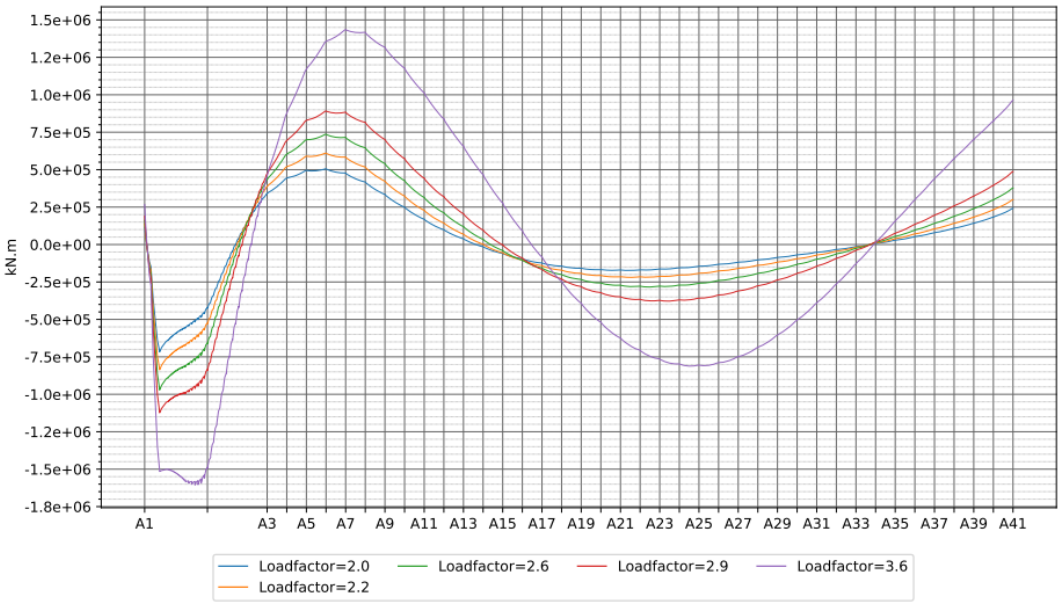

Figure 2-15: Static strong axis moment response to 10 000-year wind conditions from east, homogeneous wind distribution with labelled load factors.

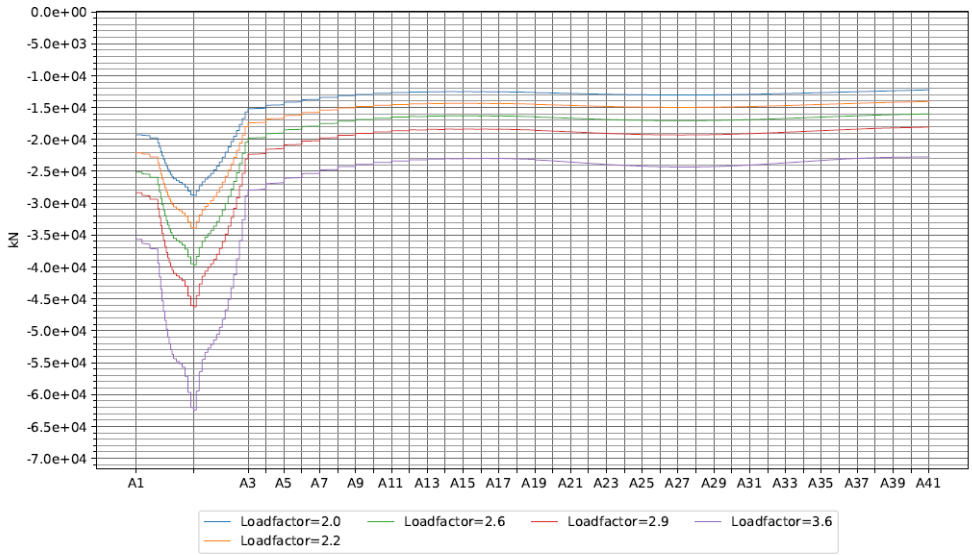

Figure 2-16: Static axial force response to 10 000-year wind conditions from east, inhomogeneous wind distribution with labelled load factors.

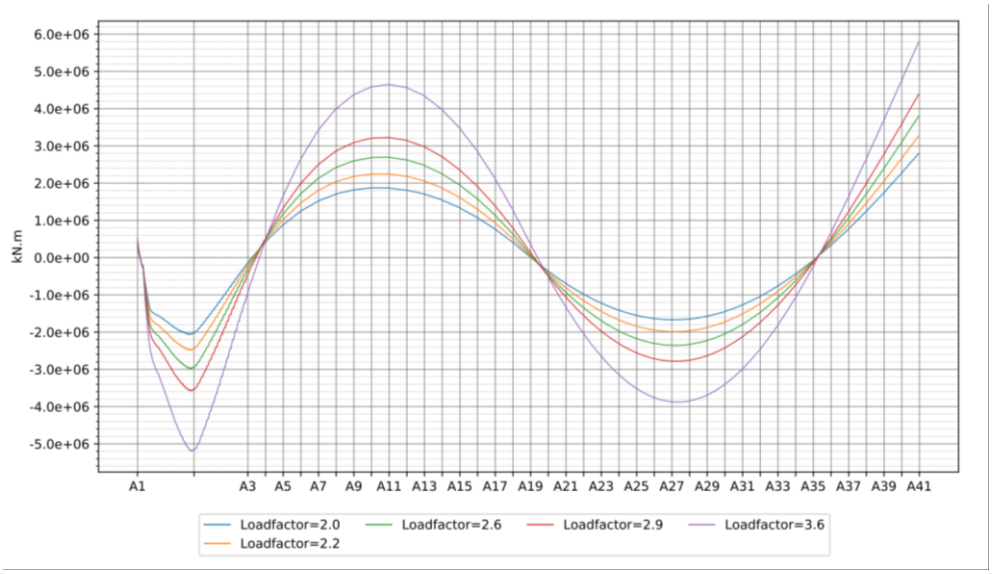

Figure 2-17: Static strong axis moment response to 10 000-year wind conditions from east, inhomogeneous wind distribution with labelled load factors.

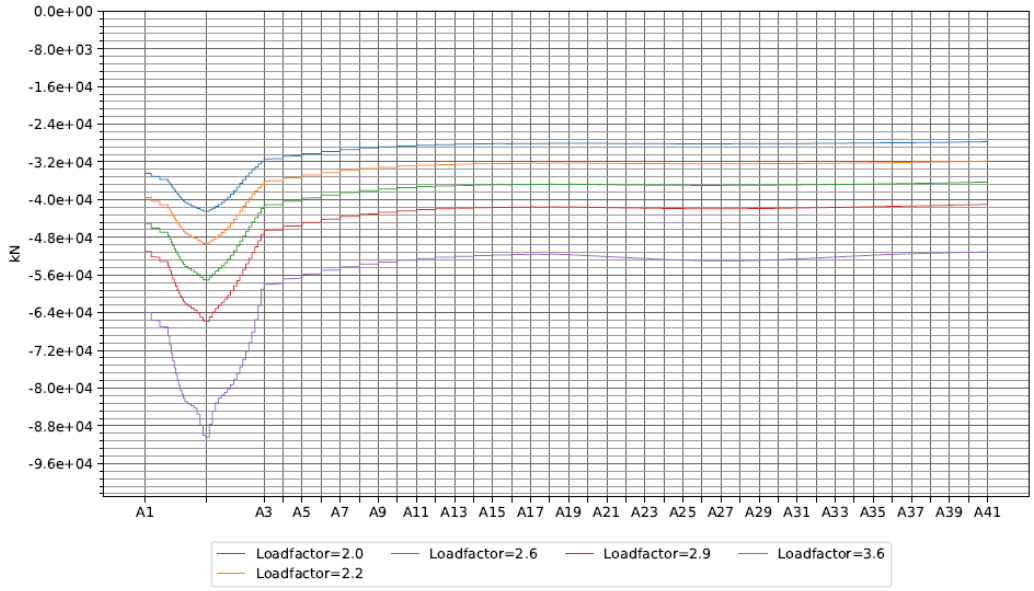

Figure 2-18: Static axial force response to 10 000-year current cross-flow condition with 10 000-year static wind from east with labelled load factors.

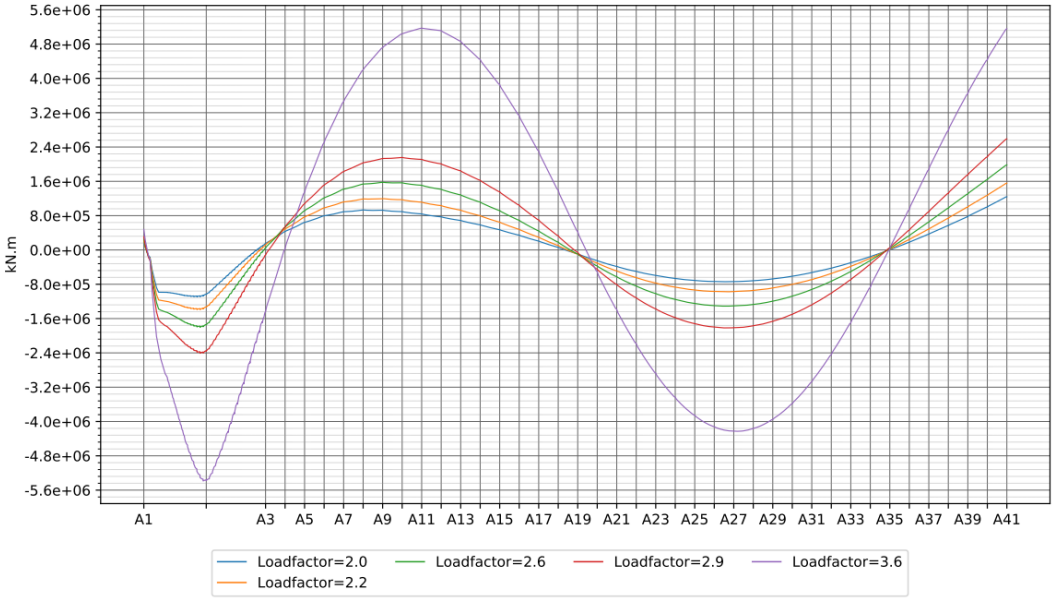

Figure 2-19: Static strong axis moment response to 10 000-year current cross-flow condition with 10 000-year static wind from east with labelled load factors.

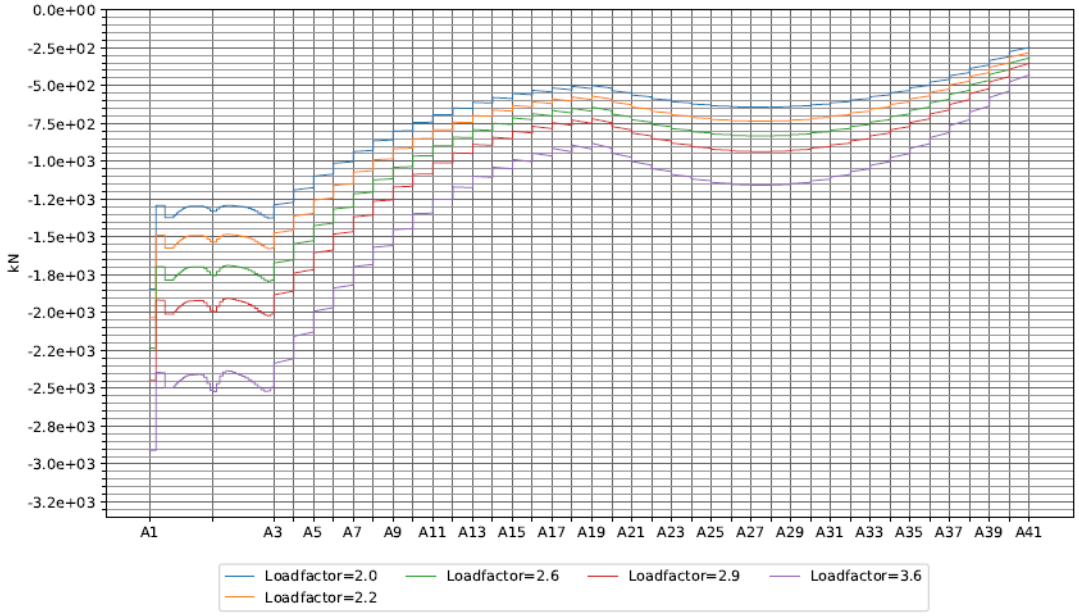

Figure 2-20: Static axial force response to 10 000-year current cross-flow condition with labelled load factors.

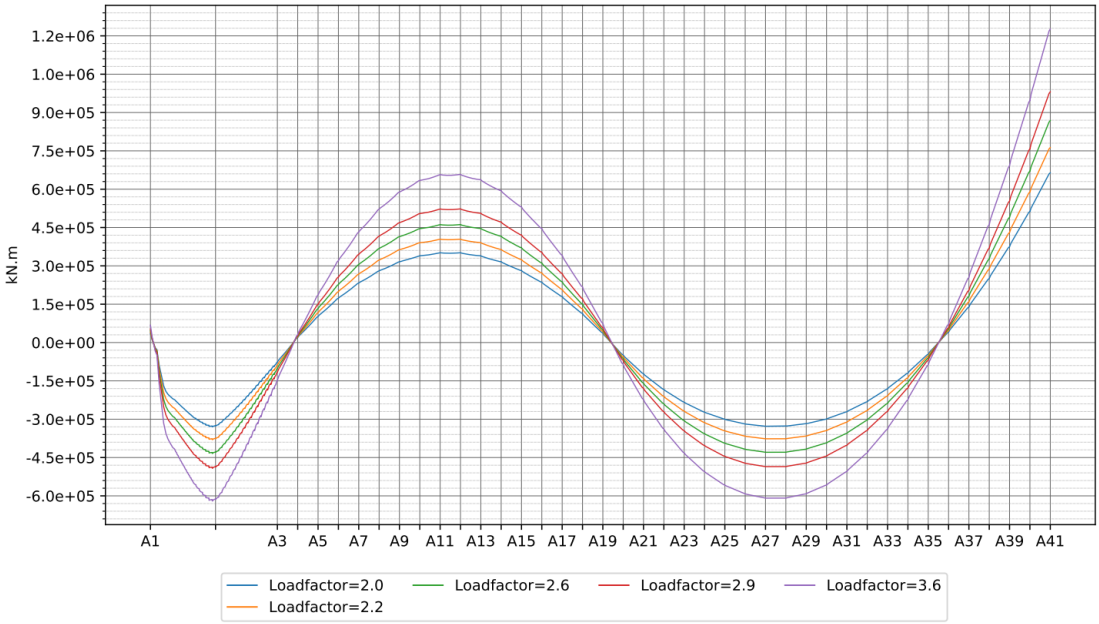

Figure 2-21: Static strong axis moment response to 10 000-year current cross-flow condition with labelled load factors.

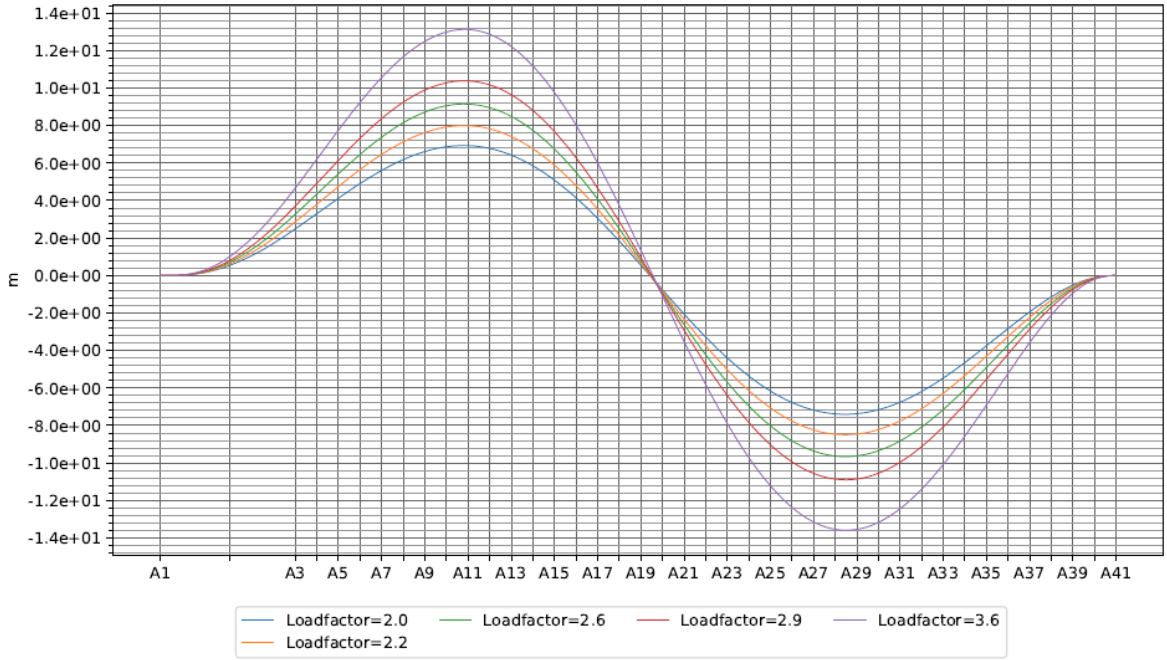

Figure 2-22: Static transverse displacement in bridge girder to 10 000-year current cross-flow condition with labelled load factors.

2.5 Combined environmental analysis

Combined global response analysis from environmental actions has been simulated dynamically in Orcaflex, in order to (i) evaluate the selected cross-sections and (ii) evaluate whether there is a significant non-linear response of the bridge. The 100-year north-western swell conditions (from 300 deg) has been applied together with the eastern wind and wind sea conditions. In addition, the 100-year cross flow condition, as presented in Figure 2-13, and permanent action are applied. Selected results are presented in Figure 2-23 - Figure 2-26. For the results labelled “load factor 2 pre-analysis”, entail that the significant wave heights has been increased by a factor 2 and the current and mean wind velocity has been increased by a factor of square root of 2. For the results labelled “load factor 2 post-analysis”, entail that the load factor has been applied post analysis.

Comparing the results for the simulations with load factors pre- and post-analysis, it is evident that the response in the bridge girder is dominated by linear effects. There is a slight increase of the static response around the tower and north abutment for the pre-applied load factor simulations, however the results are similar, overall.

Note that only the east combined load case has been considered, and the utilization may be higher for the west load cases.

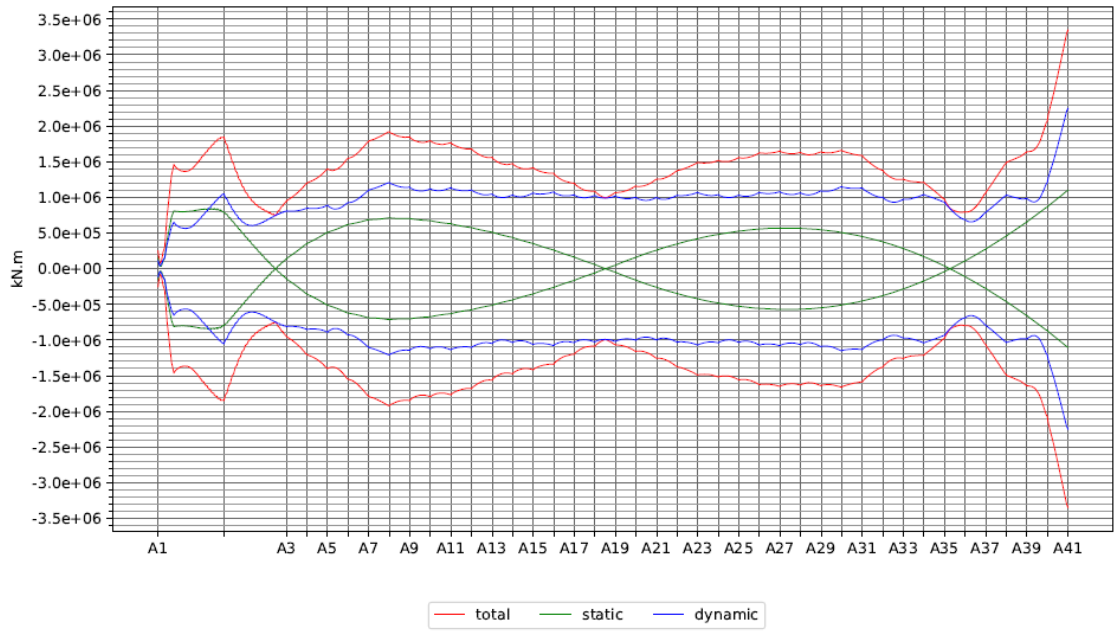

Figure 2-23: Resulting strong axis moment distribution from the combined 100-year analysis with load factor 2, applied pre-analysis.

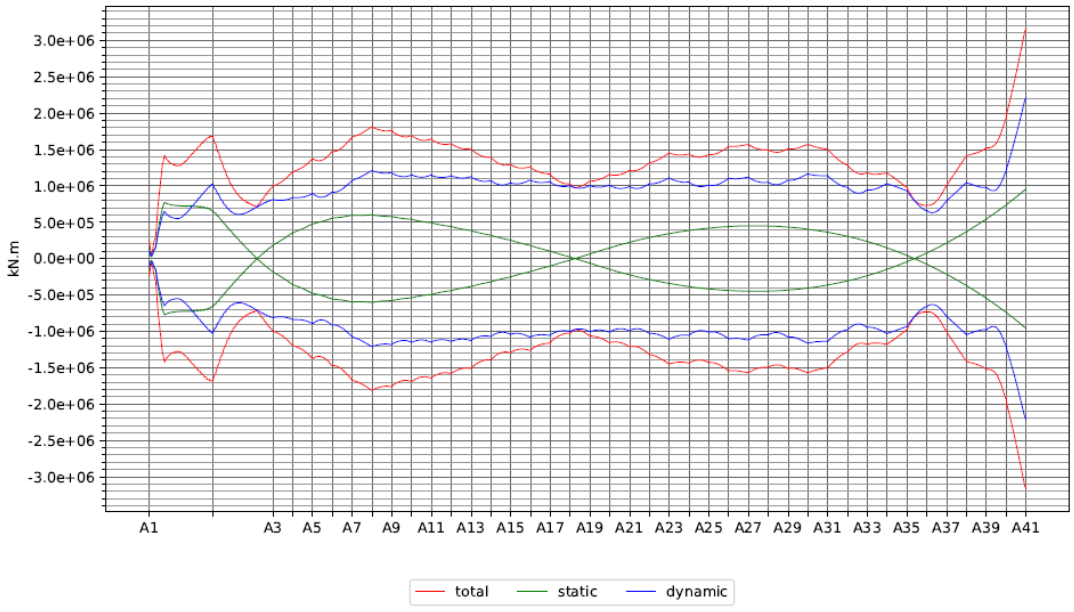

Figure 2-24: Resulting strong axis moment distribution from the combined 100-year analysis with load factor 2, applied post-analysis.

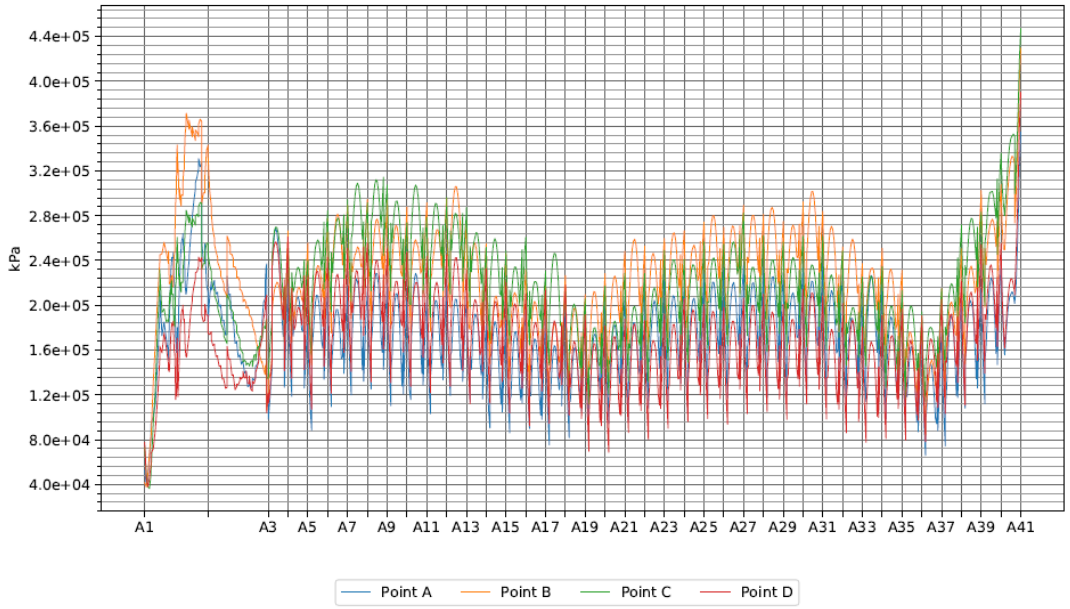

Figure 2-25: Resulting maximum von-mises stress from the combined 100-year analysis with load factor 2, applied pre-analysis. A direct von-Mises stress evaluation has been performed considering permanent, wind, swell, windsea and current action. Note that for permanent action the load factor is set to 1.2. The high utilization towards the tower is partly due to that the section modulus of section Kxx_B1 has been applied to Kxx_B2 - Kxx_B4, for simplification.

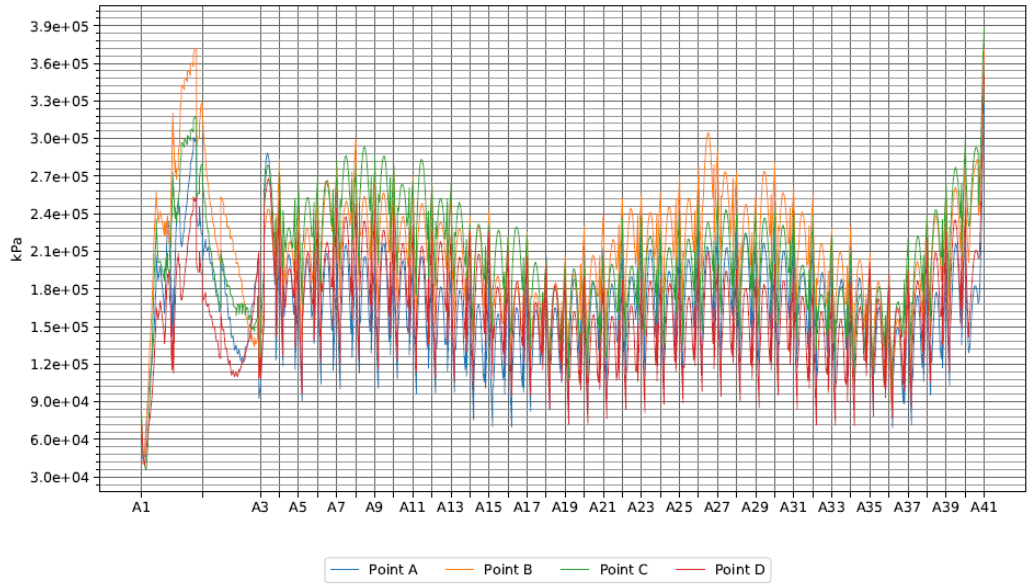

Figure 2-26: Resulting maximum von-mises stress from the combined 100-year analysis with load factor 2, applied post-analysis. A direct von-Mises stress evaluation has been performed considering permanent, wind, swell, windsea and current action. Note that for permanent action the load factor is set to 1.2. The high utilization towards the tower is partly due to that the section modulus of section Kxx_B1 has been applied to Kxx_B2 - Kxx_B4, for simplification.

2.6 Parameter study - Evaluation of damper alpha-factor in swell mode 5 conditions

To study the response for different α-values (the velocity exponent), see Section 3, a parameter study has been simulated in Orcaflex for $\alpha = [0.2,0.4,1,2]$. The damper coefficient c is held constant at 15 MNs/m. An alpha value of 1 yields the lowest response. This may be explained by the implied damping for lower α-values, which ensures locally a too high damping, such that the system is more constrained for translations at the tower position and a lower modal damping is obtained. It is expected that for lower c-values the lower alpha-factor would be more beneficial.

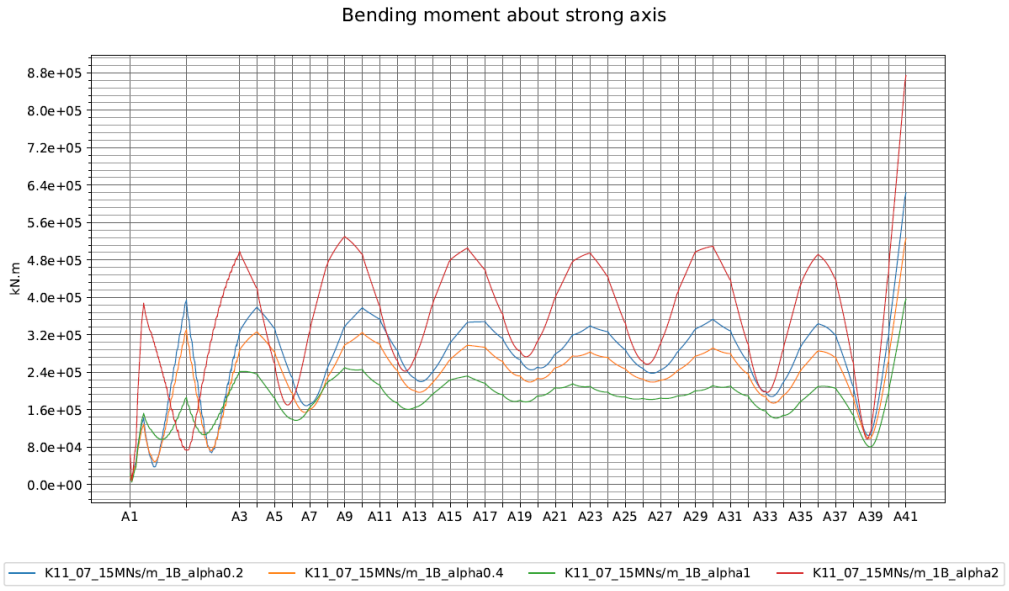

Figure 2-27: Expected maximum strong axis moment response for various α-values for damper.

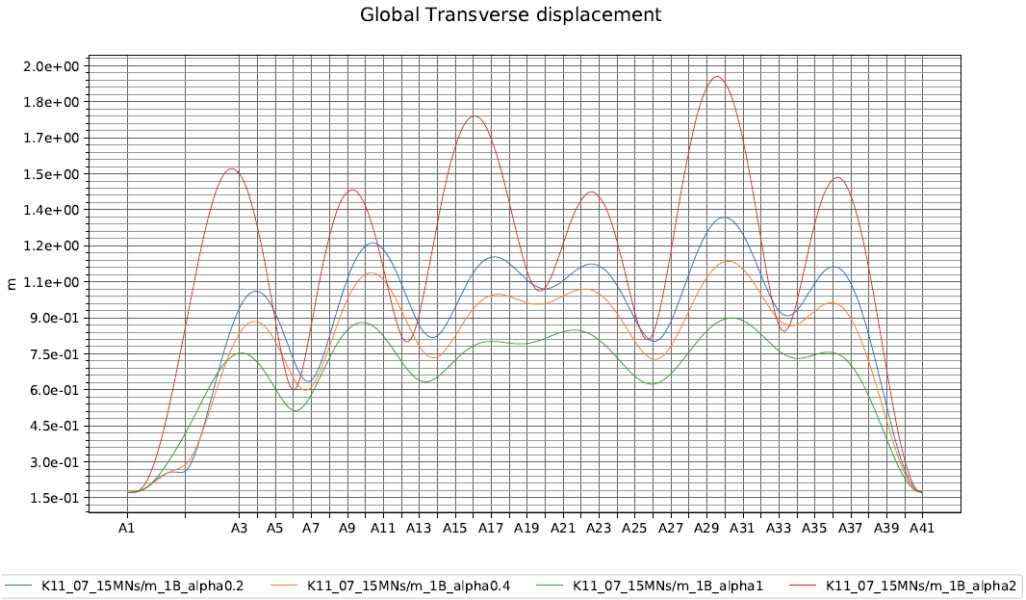

Figure 2-28: Expected maximum global transverse displacement for various α-values for damper.

3 Damper behaviour and characteristics

Traditionally, the behaviour of viscous dashpot dampers is described by the following equation (see, e.g., [1]):

$$f_d = c \cdot |\dot{u}|^{\alpha} \cdot \text{sign}(\dot{u}) \tag{2}$$

where f_d is the damping force, c is the damper constant, $\dot{u}$ is the relative velocity between the two ends of the dashpot and α is the velocity exponent. It is also common to use the less general expression:

$$f_d = c\dot{u}^{\alpha} \tag{3}$$

An unlimited range is possible for the damper constant, c, whereas the velocity exponent, α, is normally located in the range 0.3–1.0 [2]. See Attachment 8 for email correspondence with Maurer regarding possible damper specifications.

3.1 Choice of velocity exponent

The velocity exponent α affects the shape of the damping hysteresis curve, whose area describes the dissipated energy per vibration cycle. The time histories of the displacement, velocity and corresponding damping force of a generic dashpot is shown in Figure 3-1, based on a damper constant $c = 15\text{MN}/(\text{m/s})$ and a displacement amplitude of 2 m. By varying the velocity exponent, the resulting damping force is affected as shown in the figure. The resulting hysteresis loop curve, showing the functional relationship between displacement and damping force, is depicted in Figure 3-2. As seen in the figure, the dashpots with $\alpha < 0$ provide a larger energy dissipation per cycle and is thus often considered as beneficial, for the given vibration amplitude. The downside is the fact that the damping force no longer is fully out of phase ($90°$ phase shift) with the displacement response, and consequently, the restoring forces – in contrast to the case for linear viscous damping. This could possibly induce larger forces on the damper and on the structure at the position of the damper.

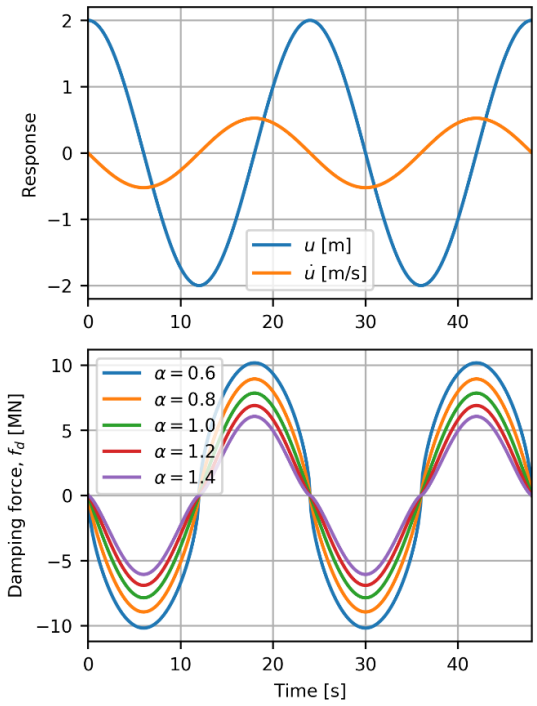

Figure 3-1: Time histories of displacement, velocity and damping force over two periods $T = 24s$, with a displacement amplitude of 2 m. The damping force is based on a damper constant $c = 15\ MN/(m/s)$ and a velocity exponent α in the range between 0.6 and 1.4.

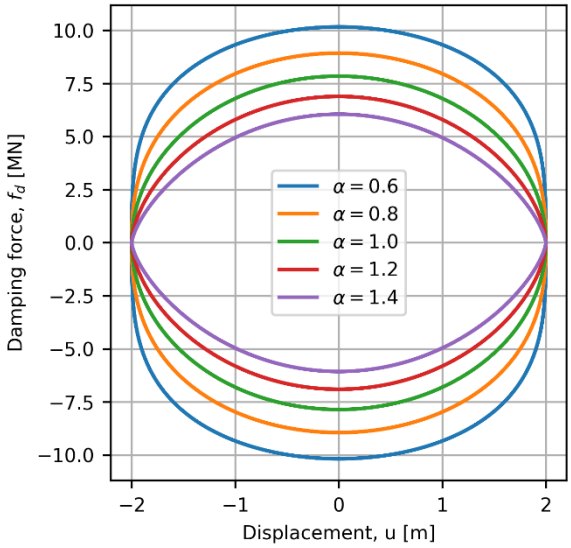

Figure 3-2: The hysteresis loop curve (force vs. displacement) corresponding to the time histories depicted in Figure 3-1

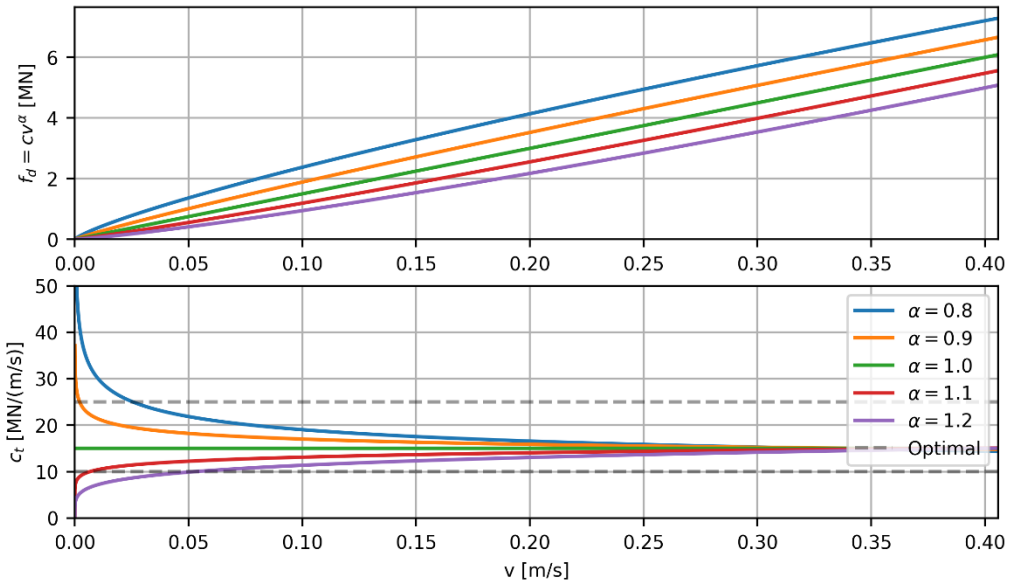

Figure 3-3: Effect of α-value on the damping force and tangent damping. $c = 15\ MN/(m/s)$ here.

By differentiating the expression in Equation 3 with respect to the velocity, the *tangent* damping constant is established, as follows:

$$c_t = \frac{df_d}{d\dot{u}} = \alpha \cdot c\dot{u}^{\alpha-1}$$

The damping force and the tangent damping constant are plotted in Figure 3-3 for velocity exponents in the range of 0.8–1.2, with $c = 15\ \mathrm{MN/(m/s)}$. An optimal range of the linear damping is given as a reference, which is defined in a qualitatively manner as a range resulting in large modal damping coefficients for modes 1–6 (see Figure 4-1–Figure 4-3). By comparison with Figure 4-1–Figure 4-3, the figure also reveals another downside of using highly non-linear dashpots; when a too low velocity exponent is applied, the structure might in effect be fixated at the damper position due to the very large tangent damping for low velocities, in turn leading to low modal damping coefficients. This effect is also demonstrated by the Orcaflex global analyses for varying α-values.

Consequently, the damper constant c must be modified to provide reasonable tangent damping constants in the relevant range of velocity.

3.2 Choice of damper constant

As the damper constant affects the complete behaviour of the system, a full analysis of the system including the dashpot damper must be conducted. This is provided in Section 4.2.

4 Modal analysis

Modal analysis has been conducted in the same manner as described in Appendix S section 3.6, and more in-depth, in Appendix F, Section 6.2. The procedure is based on the approach given in [3], and is conducted using in-house Python software combined with the modal analysis results obtained from the Orcaflex model. For the convenience of the reader, some of the details in the approach are repeated in the following sub-section.

4.1 Methodology

The modal transformation matrix $[\phi_0]$, and the modal mass $m_{n,0}$ and natural frequencies $\omega_{n,0}$ for are established using the Orcaflex model. The modes established are deliberately not including effects from hydrodynamics and are consequently termed as *dry modes*. The modal transformation matrix corresponding to the dry modes transforms generalized degrees of freedom (DOFs) $\{y\}$ to physical DOFs $\{u\}$, as follows:

$$\{u\} = [\phi_0]\{y\}$$

The elements (Einstein summation convention not implied) of the corresponding modal mass and stiffness matrices are established as follows:

$$\widetilde{M}_{0,nn} = m_{n,0}$$
$$\widetilde{K}_{0,nn} = \omega_{n,0}^2\, m_{n,0}$$

Furthermore, a modal damping (ratio of critical) ξ =0.5% is assumed, such that $C_{0,nn} = 0.5\%$. The contributions from hydrodynamics and the damper dashpots are added as follows:

$$\left[\widetilde{M}(\omega)\right] = \left[\widetilde{M}_0\right] + [\phi_0]^T[M_h(\omega)][\phi_0]$$
$$\left[\tilde{C}(\omega)\right] = \left[\tilde{C}_0\right] + [\phi_0]^T([C_h(\omega)] + [C_d])[\phi_0]$$
$$\left[\widetilde{K}\right] = \left[\widetilde{K}_0\right] + [\phi_0]^T[K_d][\phi_0]$$

where $[M_h(\omega)]$ is the added mass of all pontoons, $[C_h(\omega)]$ is the radiation damping of all pontoons, and $[C_d]$ and $[K_d]$ are the damping and stiffness matrices related to the dashpot introduced in the system. When using this formulation, it is assumed that $[M_h(\omega)]$, $[C_h(\omega)]$, $[C_d]$, and $[K_d]$ are described in the same finite element (FE) format as $[\phi_0]$, i.e., including the same DOFs. The submatrix of $[C_d]$ that describes the two DOFs connected by the dashpot, denoted i and j, is established as follows:

$$[C_d]_{i,j} = \begin{bmatrix} c & -c \\ -c & c \end{bmatrix}$$

where c is the damper constant specified. The same formulation is in principle used for $[K_d]$, but this assumed as zero for all applications herein.

The resulting system matrices are used to conduct a second eigenvalue solution, which results in a transformation matrix $[\psi]$ that transform the true generalized coordinates $\{q\}$ to dry generalized coordinates $\{y\}$, as follows:

$$\{y\} = [\psi]\{q\}$$

The physical DOFs $\{u\}$ are therefore related to the true generalized degrees of freedom (DOFs) $\{q\}$ as follows:

$$\{u\} = [\phi_0]\{y\}$$
$$= [\phi_0][\psi]\{q\}$$

This implies that the total modal transformation matrix is given as $[\phi] = [\phi_0][\psi]$. Because the system matrices are frequency-dependent, the eigenvalue problem is solved by iteration [3]. The approach given above does not introduce any assumptions about the damping in the modal analysis, in contrast to traditional modal analysis where the damping is assumed classical. Consequently, the physics of the introduction of a damper is better represented. The following results are based on including hydrodynamic contributions but disregarding aerodynamic contributions.

4.2 Modal critical damping ratios

Figure 4-1–Figure 4-3 show the estimated effect of chosen damper dashpot constant c on the critical damping ratios of modes 1–6, for the six considered back-span solutions described in the preceding sections. The damper is assumed to behave linearly in this assessment, i.e., the damping force is linear with velocity. As is observed from the figures, a damping constant maximizing the critical damping coefficient can be found for each mode and back-span configuration. This fact is supported by the fact that when the damper is larger, the resulting mode shapes change such that the damper is less mobilized; effectively, a fictious fixation is introduced. A value of c in the range $15–20\ \mathrm{MN/(m/s)}$ seems to provide a rather good damping contribution to all modes considered.

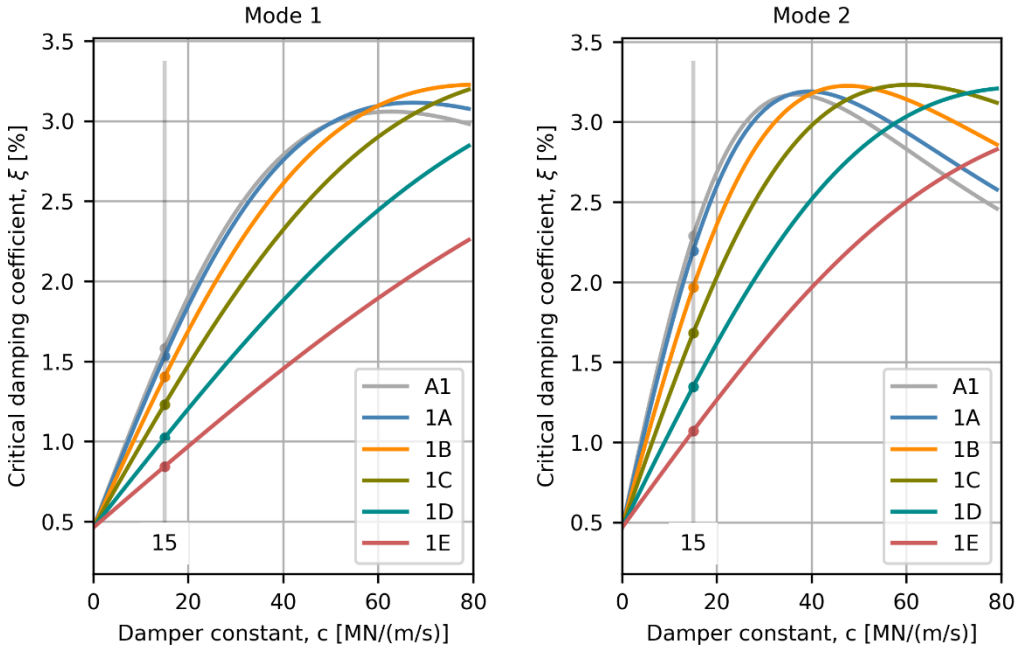

Figure 4-1: Effect of varying damper constant c for the considered back-span alternatives, for modes 1 and 2. The points on the curves corresponding to a damper constant of $c = 15\ MN/(m/s)$ are also indicated.

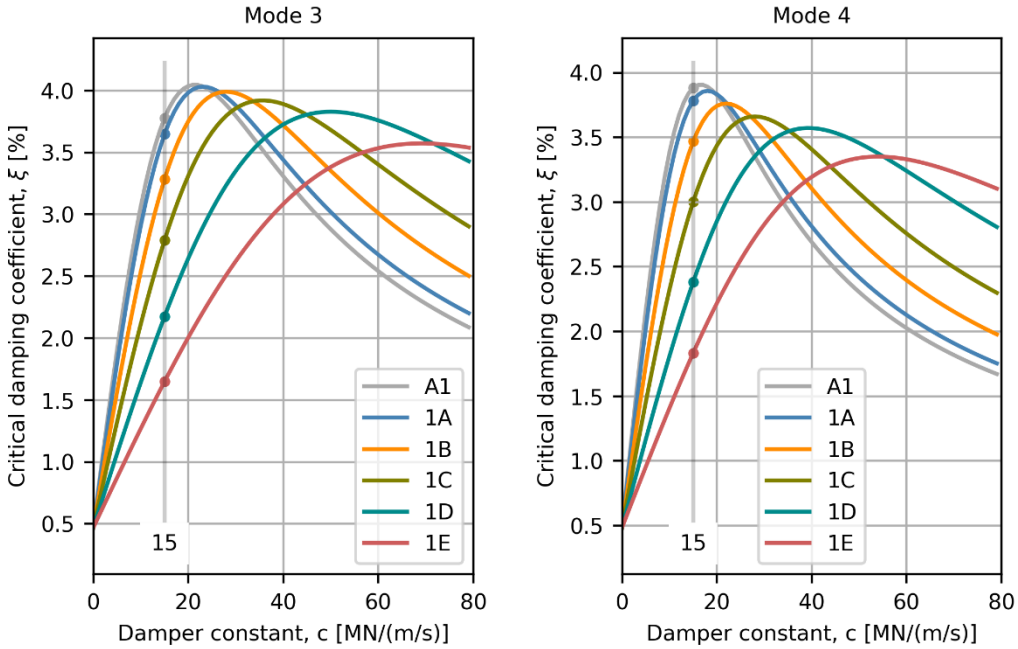

Figure 4-2: Effect of varying damper constant c for the considered back-span alternatives, for modes 3 and 4. The points on the curves corresponding to a damper constant of $c = 15\ MN/(m/s)$ are also indicated.

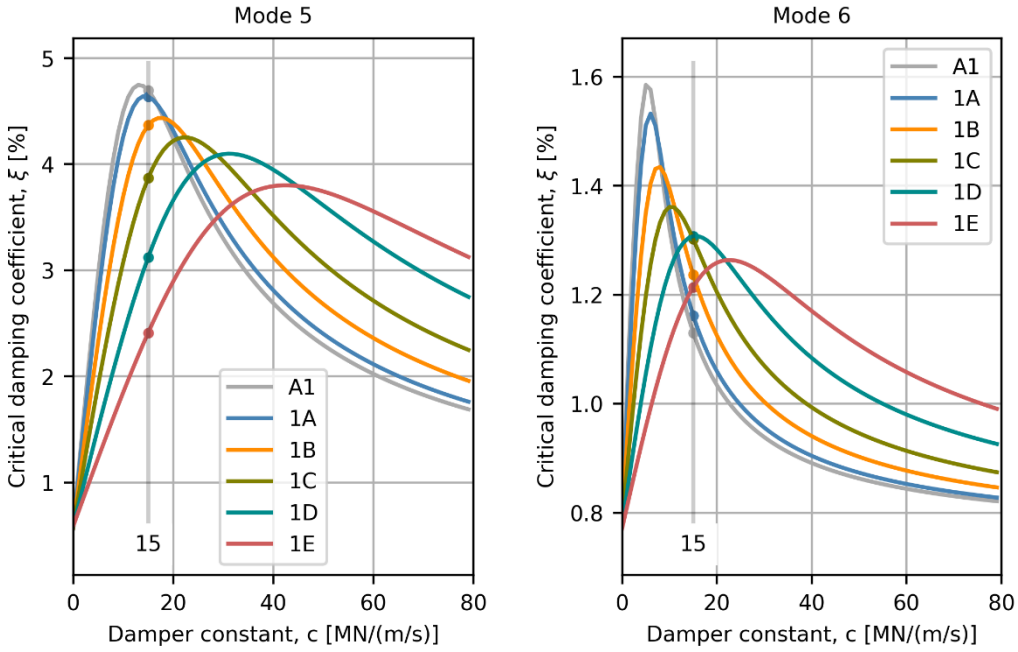

Figure 4-3: Effect of varying damper constant c for the considered back-span alternatives, for modes 5 and 6. The points on the curves corresponding to a damper constant of $c = 15\ MN/(m/s)$ are also indicated.

4.3 Validity of modal decoupling

By introducing a large non-classical damping contribution, an assessment of the complexness and coupledness of the modes should be conducted before carrying out other analyses based on the diagonalized system.

4.3.1 Modal phase collinearity

The effect of the damper with $c = 15MN/(m/s)$ on the modal phase collinearity (MPC) factor, which is described in Appendix F, Section 6.2, is illustrated by comparing Figure 4-4 and Figure 4-5. The figures also depict the critical damping ratios of shown modes. As expected, the modes have larger phase differences between response values. The MPC values are also provided in Table 5-1 and Table 5-2. For the critical mode 4, the MPC is satisfactory.

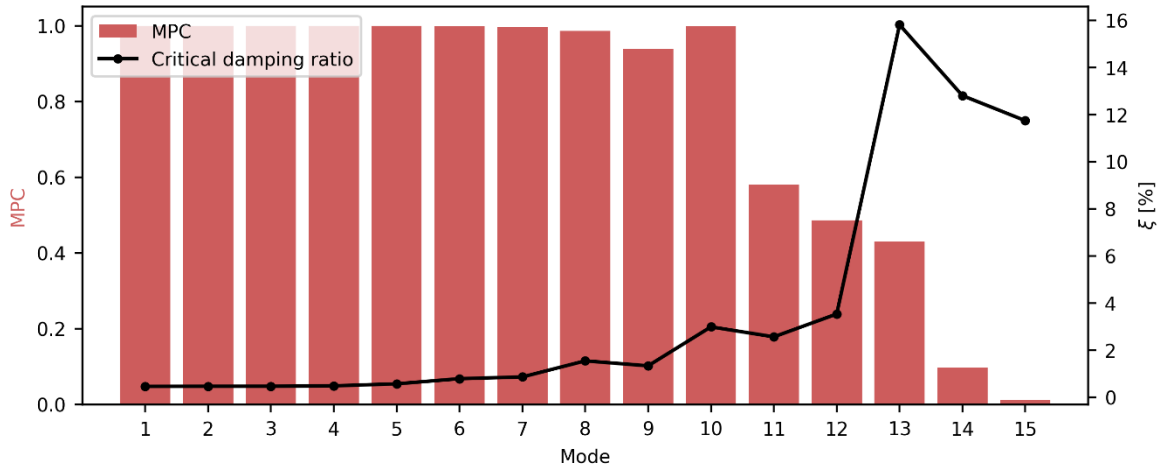

Figure 4-4: Modal phase collinearity (MPC) and critical damping ratios for the 15 first modes of the adjusted K11 model (with back-span configuration 1B) without a dashpot damper.

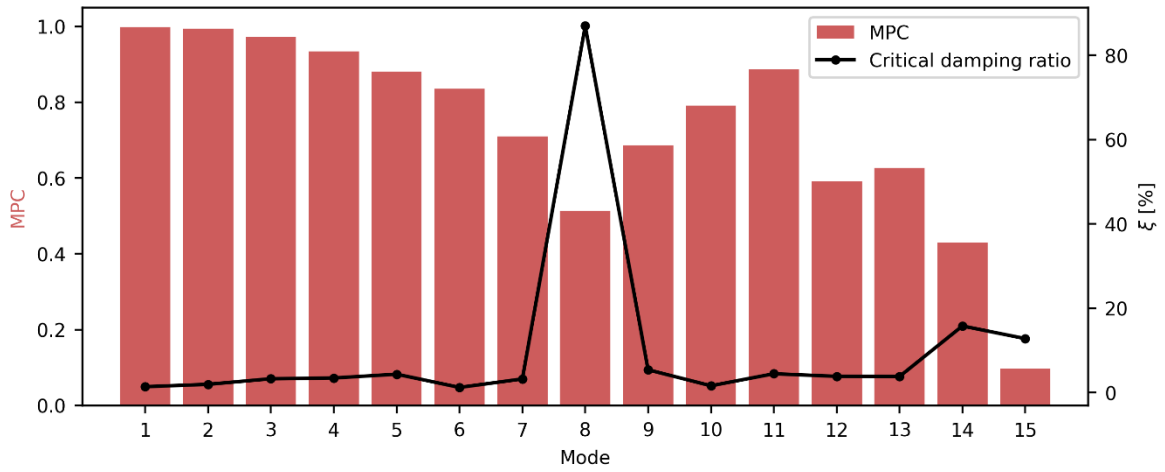

Figure 4-5: Modal phase collinearity (MPC) and critical damping ratio for 15 first modes of the adjusted K11 model (with back-span configuration '1B') with a discrete linear viscous dashpot damper with $c = 15\ MN/(m/s)$. The MPC is reduced when including the discrete damper, but is still reasonably high for the critical mode 4. Note that the axis scaling of the right-side y-axis is different from the previous figure. Also note that mode 8 of this system does not correspond to mode 8 of the undamped system.

4.3.2 Diagonality

The frequency response function (FRF) matrix, $[H(\omega)]$, can be used to construct a measure of the diagonality of the system equations, as follows:

$$\mathfrak{D}_{\mathrm{n}} = \frac{|\mathrm{diag}([\mathrm{H}(\omega_{\mathrm{n}})])|}{|[\mathrm{H}(\omega_{\mathrm{n}})]|}$$

This simply gives the ratio of the norm between the diagonal of the matrix and the full matrix at the frequencies corresponding to the damped natural frequencies of mode n. Figure 4-6 illustrates the resulting diagonality of modes 1–15. This plot supports that the diagonalization performed to assess the parametric excitation robustness of modes 1–6 is reasonable.

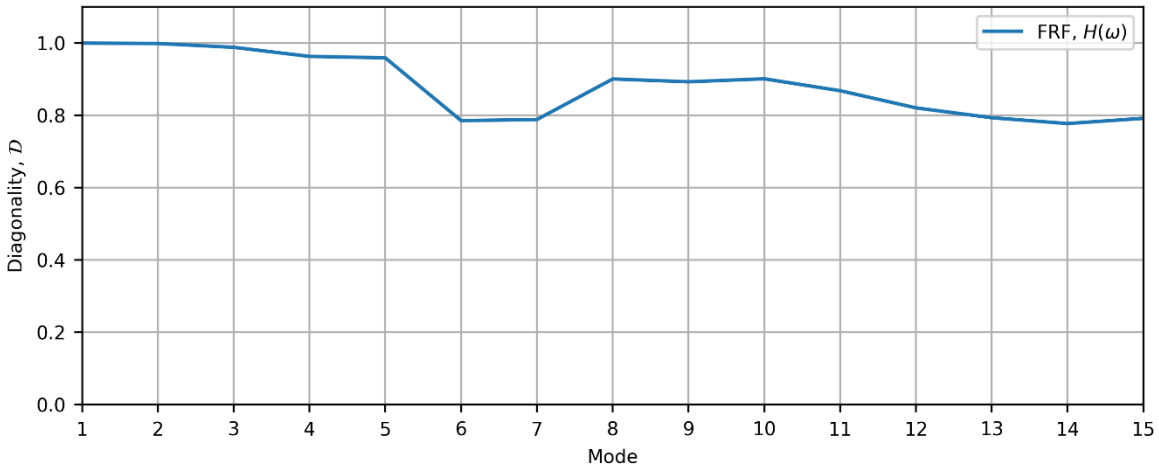

Figure 4-6: Diagonality measure, $\mathfrak{D}_n$ for the model with back-span configuration 1B and a discrete linear viscous dashpot damper with $c = 15\ MN/(m/s)$.

5 Parametric excitation

The introduction of a dashpot damper is introduced in large part to control possible parametric excitation occurring on the unanchored concept K11. The *onset criterion* states that parametric excitation will not occur if the following is satisfied [4]:

$$\sigma_N < 0.4 \cdot A_{cr}$$

where $A_{cr} = 4\xi \cdot k/\hat{k}_g$ for $\beta = 2$, i.e., when the axial force variation is applied at a frequency twice the mode being excited. Here, σ_N is the standard deviation of the axial force, $\hat{k}_g$ is the modal geometric stiffness due to a unit constant axial force in the girder, ξ is the critical damping ratio and k is the modal stiffness. It is referred to Appendix S and [4] for more details. By conducting modal analyses in line with the procedure given in Section 4.1, and diagonalizing the results (assuming that the modes are uncoupled), the robustness against parametric excitation was assessed. This is equivalent to the approach applied for the concepts K11–K14 in Appendix S. Figure 5-1 depicts the power spectral density of the axial force (approximately constant along the girder) from an Orcaflex global analysis of the bridge with back-span configuration 1B with a dashpot damper, exposed to 100-year swell conditions. Table 5-1 and Table 5-2 summarize the diagonalized modal properties of modes 1–6 for back-span configuration 1B with and without a dashpot damper, respectively. Table 5-3 summarizes the assessment of the onset criterion for back-span configuration 1B. As seen in the table, the introduction of the dashpot damper seemingly drastically improves the concept's robustness against parametric excitation. See Attachment 9 for the full assessment related to parametric excitation.

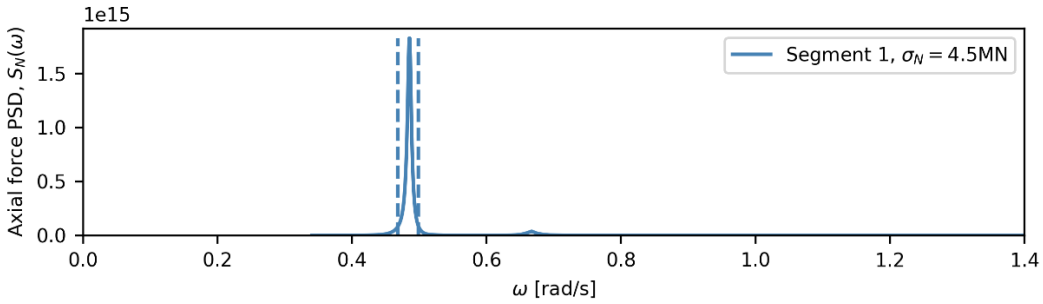

Figure 5-1: Power spectral density of axial force (close to constant along bridge girder) due to 100-year swell conditions, on K11 with backspan configuration 1B and a dashpot with damper constant $c = 15$ MN/(m/s).

Table 5-1: Summary of modes 1–6 for K11 with back-span configuration 1B, and a dashpot damper with $c = 15\ MN/(m/s)$.

Mode	T_d [s]	ξ [%]	m $[10^6 kg]$	k [MN/m]	$k/\hat{k}_g$ [MN]	A_{cr} $(\beta = 2)$ [MN]	MPC
1	114.7	1.40	82.47	0.25	73.66	4.14	0.999
2	60.8	1.97	51.81	0.55	119.51	9.41	0.994
3	34.1	3.29	60.58	2.06	203.53	26.75	0.972
4	23.2	3.47	57.66	4.25	290.75	40.35	0.934
5	16.5	4.37	28.37	4.13	433.32	75.68	0.881
6	12.9	1.24	26.75	6.34	2154.30	106.57	0.835

Table 5-2: Summary of modes 1–6 for K11 with back-span configuration 1B, without a dashpot damper.

Mode	T_d [s]	ξ [%]	m $[10^6 kg]$	k [MN/m]	$k/\hat{k}_g$ [MN]	A_{cr} $(\beta = 2)$ [MN]	MPC
1	114.8	0.46	82.77	0.25	73.77	1.37	1.000
2	61.0	0.47	52.32	0.55	119.88	2.25	1.000
3	34.5	0.47	62.97	2.08	204.88	3.85	1.000
4	23.6	0.49	62.63	4.45	290.62	5.64	1.000
5	16.9	0.57	31.52	4.34	425.39	9.73	1.000
6	13.0	0.79	30.77	7.15	1142.67	36.06	0.998

*Table 5-3: Assessment of onset criterion. *) No results available for c=0, so results from c=15 MN/(m/s) are used.*

Backspan config	Damper constant, c [MN/(m/s)]	β (load vs. mode 4)	σ_N [MN]	$\sigma_N/0.4$ [MN]	A_{cr} $(\beta = 2)$ [MN]	Onset criterion, $\frac{\sigma_N}{0.4} < A_{cr}$
1B	0	1.82	4.5*	11.26	5.64	Fails
1B	15	1.79	4.5	11.26	40.35	OK

6 List of attachments

Attachment 1: Eigenmodes

Attachment 2: Combined von mises design check, load factor pre- and post.

Attachment 3: Static analysis, for evaluation of static resistance to buckling.

Attachment 4: Parameter studies, swell

Attachment 5: Windsea results

Attachment 6: Parameter studies, wind

Attachment 7: Load RAOs

Attachment 8: Mail correspondence Maurer

Attachment 9: Complete results for evaluation of parametric excitation.

References

[1] A. Bahnasy and O. Lavan, “Linear or nonlinear fluid viscous dampers? A seismic point of view,” in *Structures Congress 2013: Bridging Your Passion with Your Profession*, 2013.

[2] D. Lee and D. P. Taylor, “Viscous damper development and future trends,” *The Structural Design of Tall Buildings,* vol. 10, no. 5, pp. 311-320, 2001.

[3] K. A. Kvåle, R. Sigbjörnsson and O. Øiseth, “Modelling the stochastic dynamic behaviour of a pontoon bridge: A case study,” *Computers & Structures,* pp. 123-135, 2016.

[4] O. Øiseth, B. Costa and A. Fenerci, “Dynamic stability of elastic nonlinear systems subjected to random excitation (SBJ-32-C4-NTNU-22-RE-001),” SVV/NTNU, 2018.